

## **Section 1**

**Atmospheric data assimilation  
schemes, analysis and initialization,  
data impact studies, observing system  
experiments**



# Use of CAMEX data sets in an Adaptive Observational Strategy for Hurricane Forecasts

*Mrinal K. Biswas and T. N. Krishnamurti*

*The Florida State University  
Tallahassee, FL 32306-4520, USA  
[biswas@earl.met.fsu.edu](mailto:biswas@earl.met.fsu.edu)*

## 1. Introduction

Ensemble studies have shown that error arising from an NWP model is not homogeneous in space. The predictions will be more sensitive in some areas as compared to others. Earlier researchers have found out that the uncertainty in the initial conditions is mainly responsible for forecast errors. A very high resolution realtime observational system will be very expensive and impractical. The identification of areas from where the analysis errors are large and is bound to play a significant role in the improvement of forecasts. Zhang and Krishnamurti (2000) proposed a simple method that could provide some guidance for aircraft reconnaissance missions to aid hurricane observations.

## 2. Methodology

This was based on the mapping of the spread of forecast errors from the construction of the variance of a 50-member ensemble with respect to a control run. The variables at locations of maximum variance were back correlated to a 12 hr forecast field (or to a near time field) to locate regions where the errors emanate due to data uncertainties. A next step in the analysis is to introduce new data sets within that targeted area of high correlations. In the present study CAMEX 3 LASE and Dropsondes data sets are used to study the impact of the data using the Adaptive observational strategy. Those targeted data sets are assimilated with those of the control run to obtain a new data analysis.

This appears to be a very powerful strategy for the deployment of adaptive observations.

## 3. Results and Conclusions

We next illustrate the results from one experiment for hurricane Georges (1998). The control initial states for these experiments were obtained from the operational analysis of ECMWF.

Fig (1a) illustrates the distribution of the variances of forecasted deep layer mean geopotential heights calculated from the ensemble spread of 50 forecast experiments (forecasts of 48 hour duration). These variances cover a region in the vicinity of the hurricanes where the storm was expected to move to in 48 hours. A large spread was noted and this suggests that model forecasts have a considerable sensitivity to the initial states.

The field of back correlation for Georges is illustrated in fig 1b. These are analyzed to locate regions of large correlations that signify possible regions from where the error spread emanates. This identifies a region for targeted observations. Special observations of humidity, wind and temperature (over these region of high back correlations) are assimilated using 3DVAR along with those of the control run data sets to prepare for the adaptive observation based forecast experiments. Fig 1c shows the impact of the new data sets in the area where the back correlation was  $\geq 0.6$ . The Initial time (I), the targeted time (T) and the verification time (V) best track position are shown in the plots for reference. The strength of this study is on the rather simple strategy for the

deployment of adaptive observations that have been presented here. The dropsonde plus LASE (D+L) data sets clearly shows a marked improvement over the control experiment which consists of only conventional data.

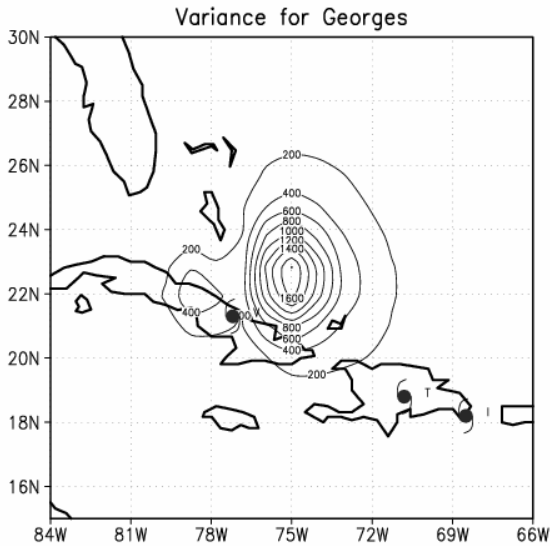


(Figure 1a)

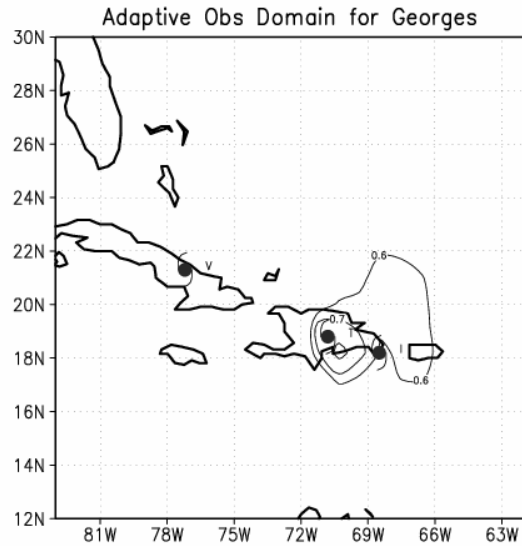


(Figure 1b)

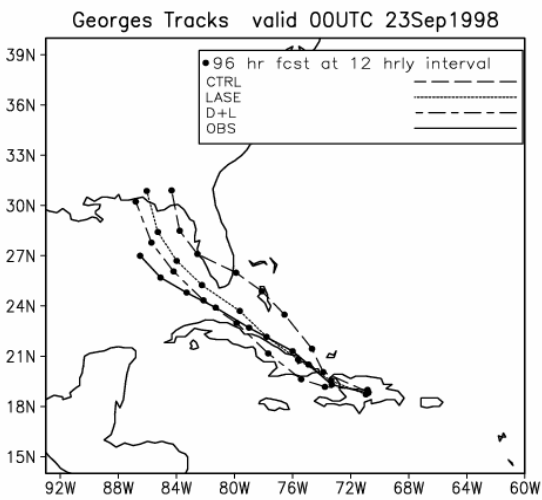


(Figure 1c)

Figure 1. (a) Forecast error variance field for Georges at 12UTC 24 September 1998. (b) Back correlation field valid 00UTC 23 September 1998. (c) 96 hour forecast at 12 hourly interval starting 00UTC 23 September 1998. CTRL - control forecast, LASE- forecast with only LASE data assimilated, D+L - forecast with Dropwindsondes+LASE data assimilated. The observed (OBS) best track positions are plotted for reference.

The Adaptive observational Strategy, outlined above, has been tested extensively for hurricane forecast improvements (Zhang and Krishnamurti, 2000 and Biswas and Krishnamurti 2005).

**References:**

Biswas, M. K. and T. N. Krishnamurti, 2005: Adaptive Use of Research Aircraft Data Sets for Hurricane Forecasts, *Submitted to Weather and Forecasting*.  
 Zhang, Z., and T.N. Krishnamurti, 2000: Adaptive observations for hurricane prediction. *Meteorol. Atmos. Phys.*, **74**, 19-35.

# Use of QuikSCAT wind observations in the assimilation and forecasting system of DWD

Alexander Cress, Christina Köpken, Heinz Werner Bitzer  
Deutscher Wetterdienst, P.O. BOX 106465, Offenbach am Main, Germany

Space-borne scatterometer data provide accurate near surface wind observations (both wind speed and direction) over the global oceans with high temporal and spatial resolution under most weather conditions. With an intensification of usage of satellite data at the German Weather Service (DWD), the implementation of wind observations from Seawinds scatterometer onboard the QuikSCAT satellite is being worked on. QuikSCAT has a swath of 1.800 km, although only the inner 1400 km is illuminated by both beams and approximately 90% of the earth surface is covered by the instrument in one day.

Current assimilation tests use the wind vector retrievals provided by JPL. Prior to assimilation experiments an extensive monitoring was carried out to determine quality criteria and any needed bias correction. The wind vector retrievals at a resolution of 25 km are thinned to a resolution of 50 km, roughly in match with the operational model resolution of 40 km. Duplicate and incomplete records are filtered out of the observation handling process and sea ice and land contaminated wind data are excluded. As, unfortunately, the Ku-band scatterometer is very sensitive to rain contamination, a careful elimination of poor quality rain contaminated data is necessary. For this purpose, the performance of the rain flagging algorithm developed at KNMI (Portabella and Stoffelen, 2002) in the framework of OSI-SAF has been compared with the JPL rain flag (Huddleston and Styles, 2000) provided within the data. Data monitoring results show, that the KNMI rain flag is mostly able to flag poor quality scatterometer data, whereas the JPL rain flag additionally eliminates many winds in rainy areas which seem of acceptable quality. This is especially obvious in regions of extreme weather conditions, like e.g. tropical cyclones. Additionally, a bias correction of wind speed is applied before assimilating the data, since data monitoring indicates dependencies of biases both on wind speed and rain probability. The beneficial impact of rain-flagging, elimination of land/sea contamination and bias correction on the data quality is depicted in Figure 1. By using the extensive quality control mechanisms described above, the correlation between QuikSCAT wind speeds and collocated model first guess wind speeds increases from 0.65 to 0.82.

The assimilation of QuikSCAT data, tested in the currently operational OI analysis scheme, have a positive impact on the analyses performance, especially in cases of tropical cyclones, where the position and strength of the investigated cyclones are improved. Unfortunately, a lot of winds around the center of the cyclones are rain-contaminated and therefore cannot be used, which reduces the impact of QuikSCAT wind data considerably. Also, the first guess wind check occasionally rejects correct wind data in severe weather systems, where wind speed and direction varies considerably over short distances. Here, an adapted formulation is necessary in the future and further advantages will be offered within the 3DVAR analysis system currently under development. The overall impact of the QuikSCAT wind observations on the forecast quality of the global forecasting system of DWD is positive on the Southern Hemisphere for up to 72 hours (Figure 2), slightly negative later on in the forecast and slightly negative on the Northern Hemisphere.

## References

Hudleston, J.N., and Stile, B.W., 2000: A Multi-dimensional Histogram Technique for flagging rain contamination on QuikSCAT. Proc. of IEEE International Geoscience and Remote Sensing Symposium, Vol. 3, pp. 1232-1254

Portabella, M., and Stoffelen, A., 2002: Quality Control and wind retrieval for SeaWinds. Final report of the EUMETSAT QuikSCAT fellowship, KNMI, de Bilt, the Netherlands.

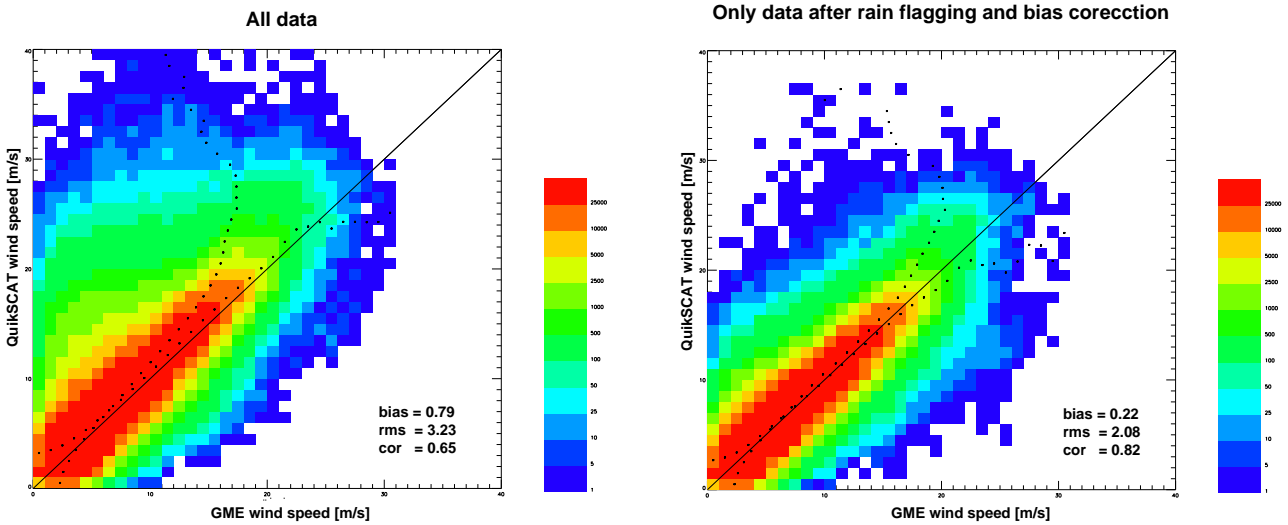


Figure 1: Scatter plots between QuikSCAT wind speeds and collocated GME first guess wind speeds for all data (left panel) and for bias corrected wind speed data that were not rejected due to rain contamination (right panel).

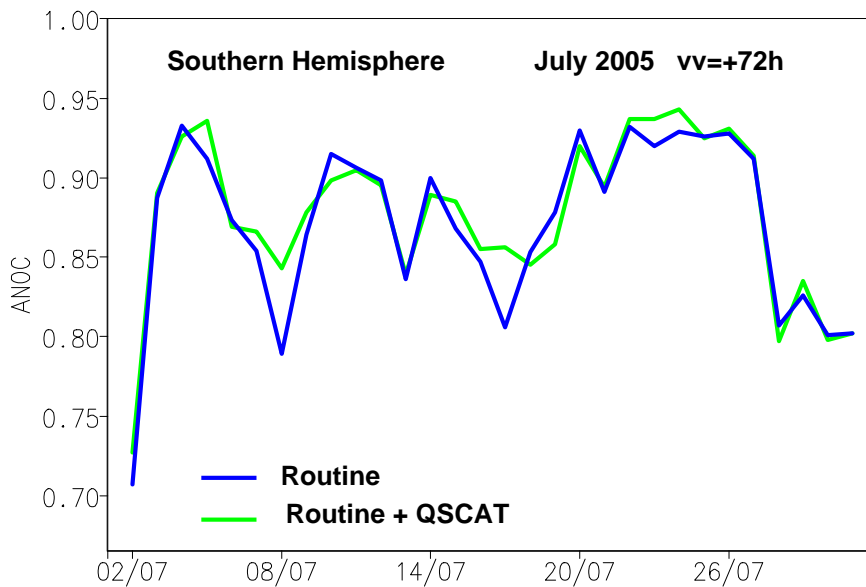


Figure 2: Time series of anomaly correlation coefficients of the sea surface pressure for the Southern Hemisphere at forecast time of 72h for control (red) and experiment (green) forecasts, using QuikSCAT wind observations, from July 02 to July 30, 2005 00 UTC.

## Marine Wind Retrieval in Non-Precipitating Regions Using Synthetic Aperture Radar

Richard Danielson<sup>1</sup>, Michael Dowd<sup>1</sup>, and Harold Ritchie<sup>1,2</sup>

<sup>1</sup>Dalhousie University, Halifax NS, Canada

<sup>2</sup>Meteorological Research Branch, Dorval QC, Canada

Forecasts that are made using the Global Environmental Multiscale (GEM) model are produced operationally at the Canadian Meteorological Centre on a 15-km grid and even higher resolution regional runs are being examined. Such forecasts contain small-scale wind features that appear realistic, but evaluating the accuracy with which these features can be modeled and predicted with in situ observations would be prohibitively expensive. Advanced observational platforms, such as Radarsat-1, provide a high resolution reference. However, the backscatter cross section from this synthetic aperture radar (SAR) depends not only on the wind field, but on other physical processes as well. In order to evaluate a model forecast, it is necessary to gauge the accuracy of the SAR data and the marine winds derived from them.

Errors in SAR and GEM data can be explicitly considered from a regression perspective. The regression equations for SAR backscatter cross section ( $y$ ) and the GEM zonal and meridional wind components ( $x^b$ ) can be written (in column matrix form) as

$$y = \alpha^{-1}[CMOD(\mathbf{x}) + \mathbf{e}_y]$$

$$\mathbf{x}^b = \mathbf{x} + \mathbf{e}_x$$

where the errors are  $\mathbf{e}_y$  and  $\mathbf{e}_x$  and  $\mathbf{x}$  denotes the wind field to be estimated. The parameter  $\alpha$  depends linearly on incidence angle and permits bias in multi-beam SAR acquisitions (cf. Vachon et al 1997) to be accounted for. The CMOD operator defines an empirical relationship between the wind field and the radar cross section (Hersbach 2003). It is a function of the SAR beam incidence angle, wind speed, and wind direction (relative to the satellite look angle). This relationship has been tuned using the ERS C-band scatterometers, whose polarization is vertical for send and receive. Because the Radarsat SAR polarization is horizontal, we include a polarization correction following Vachon and Dobson (2000). SAR observation errors (both radiometric and geometric, with the latter including errors in incidence angle) are resolved in the  $\mathbf{e}_y$  term, as are errors in CMOD and its polarization correction.

The regression equations are nonlinear owing to CMOD. Following Dowd et al. (2001), we derive from the regression equations a nonlinear cost function

$$J(\mathbf{R}, \mathbf{x}) = \ln|\mathbf{R}| + [CMOD(\mathbf{x}) - a\tilde{y}]^T \mathbf{R}^{-1} [CMOD(\mathbf{x}) - a\tilde{y}] +$$

$$\ln|\mathbf{B}| + [\mathbf{x} - \mathbf{x}^b]^T \mathbf{B}^{-1} [\mathbf{x} - \mathbf{x}^b]$$

which assumes a log likelihood form for the errors. Here, the  $\mathbf{R}$  and  $\mathbf{B}$  matrices are the error covariance matrices of the SAR observations and the model winds, respectively. The two terms on the rhs involving  $\mathbf{x}$  are measures of the variance of the SAR and GEM errors, respectively (Seber and Wild 1989). The tilde over the SAR observations indicates that we have removed the incidence angle dependence of these data using CMOD. This allows  $\mathbf{R}$  to be positive definite. The cost function  $J$  is generally a function of the estimated winds

( $\mathbf{x}$ ) and the *unknown* error covariances ( $\mathbf{R}$  and  $\mathbf{B}$ ). We assume that these decay exponentially with a length scale of 150 km and  $\mathbf{B}$  error variances are fixed at  $1 \text{ m}^2/\text{s}^2$  (i.e., only  $\mathbf{R}$  varies).

We employ 609 SAR acquisitions from June 2004 to July 2005 at 6.4-km resolution and interpolate the 15-km GEM model wind and precipitation forecasts to this resolution. (A forecast spinup of at least 6 hours is allowed first.) Ship and buoy observations within 90 minutes and 50 km of these acquisitions are used to validate the resulting wind fields. If the SAR observations are used to validate the retrieved SAR backscatter, then we find a bias of 0.3 dB in both the GEM and retrieved errors. There is also a reduction in the corresponding standard deviation from 1.49 dB (GEM) to 1.33 dB (retrieved), which is to be expected. The independent comparison in terms of wind speed and direction employs the ship and buoy winds, but little evidence is found for reductions in bias and standard deviation. Improved representations of  $\mathbf{R}$  and  $\mathbf{B}$  are being examined.

Distinctions between regions with and without precipitation (according to the GEM forecasts) and between SAR data taken at low and high incidence angles have also been examined. Triple collocations (where SAR, GEM, and in situ data are all valid) that contain precipitation are found to have slightly higher wind speed error standard deviation than collocations without precipitation (3.4 m/s versus 2.1 m/s; however, note that the precipitation regions also have slightly stronger wind speeds). Triple collocations with no precipitation and low incidence-angle SAR data are also found to have higher wind speed error standard deviation than for the high incidence-angle collocations (2.5 m/s versus 2.2 m/s, respectively). These results indicate that a 2D-variational approach to quantifying SAR (and GEM) errors is instructive. They also suggest how improvements in the  $\mathbf{R}$  and  $\mathbf{B}$  error covariance matrices might be made.

## References

- Dowd, M., P. W. Vachon, F. W. Dobson, and R. B. Olsen, 2001: Ocean wave extraction from RADARSAT synthetic aperture radar inter-look image cross-spectra. *IEEE Trans. Geosci. Remote Sens.*, **39**, 21-37.
- Hersbach, H., 2003: CMOD5: An improved geophysical model function for ERS C-band scatterometry. ECMWF Tech. Memo. 395, 50 pp.
- Seber, G., and C. Wild, 1989: **Nonlinear Regression**. Wiley, New York, 792 pp.
- Vachon, P. W., and F. W. Dobson, 2000: Wind retrieval from RADARSAT SAR images: Selection of a suitable C-band HH polarization wind retrieval model. *Can. J. Remote Sens.*, **26**, 306-313.
- Vachon, P. W., A. L. Gray, C. E. Livingstone, and A. P. Luscombe, 1997: Adaptive compensation of RADARSAT SAR analogue-to-digital converter saturation power loss, International Symposium on Geomatics in the Era of RADARSAT (GER '97), Ottawa, Canada, May 25-30, 1997.

## Diagnosis of error statistics in observation space

G. Desroziers, L. Berre, B. Chapnik and P. Poli

Météo-France, Centre National de Recherches Météorologiques  
Toulouse, France

Most main operational assimilation systems are now based on the variational formalism (Lewis and Derber 1985; Courtier and Talagrand 1987, Rabier *et al* 2000). Such a formalism allows the use of a large spectrum of observations and in particular satellite data that are not directly and linearly linked with model variables. However, those variational algorithms still rely on the theory of least-variance linear statistical estimation. In the linear estimation theory, each set of information is given a weight proportional to the inverse of its specified error covariance. The pieces of information are classically given by observations and a background estimate of the state of the atmospheric flow. Analysis systems are then dependent on appropriate statistics for observation and background errors. Unfortunately those statistics are not perfectly known and their determination remains a major challenge in assimilation systems.

One source of information on the observation and background errors is contained in the statistics of the innovations, that is the differences between observations and their background counterparts (Hollingsworth and Lönnberg 1986, Andersson 2003).

On the basis of linear estimation theory (Talagrand 1997), it can be shown (see Desroziers *et al*, 2006) that simple consistency diagnostics should be fulfilled in an optimal analysis. These diagnostics can potentially provide an information on imperfectly known observation and background error statistics. Another advantage of these diagnostics is that they are nearly cost-free and can be applied to any analysis scheme.

The application of the computation of the diagnostics on analyses issued from the operational French 4D-Var system shows likely diagnosed values for observation and background errors (see Fig. 1). Even if the values of background errors cannot be directly used in model space assimilation scheme, the study of these errors can be quite useful to understand the relative impact of observations in the analysis for observations that are not directly related to the state variables. This is in particular the case for satellite data for which the diagnosed errors can also be compared to randomized estimates of background errors. Since the observation operator includes the model integration in a 4D-Var scheme, the proposed diagnostic can be similarly used to diagnose the implicit evolution of background errors in 4D-Var.

Furthermore, it can be shown that it is possible to adapt the values specified in an analysis scheme by an iterative method. This can be useful to adapt observation errors but also background errors in observation space that are classically used in the first-guess check control of observations.

The use of such consistency diagnostics also seems to be a promising way to tackle the problem of the estimation of correlation between observation errors.

Another domain of interest is the use of the diagnostic of estimation error in observation space that will have to be investigated in the future.

Nevertheless, such diagnostics also have to be well understood at the same time from a theoretical and practical point of view. In particular it can be

shown that a spectral vision can be helpful in this perspective, by highlighting the role of a scale separation between background and observation errors.

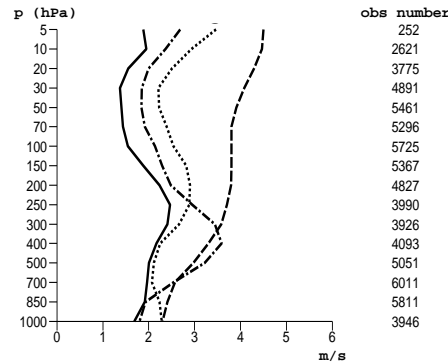


Figure 1: Vertical profiles of diagnosed square-roots of background (solid line) and observation errors (dotted line) for wind radiosonde observations in Northern Hemisphere, compared to profiles of corresponding specified variances of background (dash-dot line) and observation errors (dashed line). All values are in m/s. The numbers of observations used to compute statistics are indicated on the right side of the figure.

## References

- [1] E. Andersson. Modelling of innovation statistics. pages 153–164, 2003. Proceedings of the ECMWF Workshop on Recent Developments in Data Assimilation for Atmosphere and Ocean, Reading, September 2003.
- [2] P. Courtier. Application du contrôle optimal à la prévision numérique en météorologie, 1987. Thèse de doctorat de l’Université Paris VI, 252 pp.
- [3] G. Desroziers, L. Berre, B. Chapnik, and P. Poli. Diagnosis of observation, background and analysis error statistics in observation space. *Quart. J. Roy. Meteor. Soc.*, 2006. In press.
- [4] A. Hollingsworth and P. Lönnberg. The statistical structure of short-range forecast errors as determined from radiosonde data. part I: The wind field. *Tellus*, 38A:111–136, 1986.
- [5] J. M. Lewis and J. C. Derber. The use of adjoint equations to solve a variational adjustment problem with advective constraints. *Tellus*, 37A:309–322, 1985.
- [6] F. Rabier, H. Järvinen, E. Klinker, J.-F. Mahfouf, and A. Simmons. The ECMWF operational implementation of four-dimensional variational assimilation. I: Experimental results with simplified physics. *Quart. J. Roy. Meteor. Soc.*, 126:1143–1170, 2000.
- [7] O. Talagrand. Assimilation of observations, an introduction. *J. Met. Soc. Japan*, 75:191–209, 1997.

# Operational use of Satellite Radiances at Deutscher Wetterdienst

Reinhold Hess, Christoph Gebhardt  
Deutscher Wetterdienst (DWD), Research and Development  
D-63067 Offenbach, Germany, January 5, 2006  
reinhold.hess@dwd.de

The operational use of satellite radiances of the polar orbiting satellites has changed at DWD on 4 January 2005. Hitherto satellite products (SATEMS) were assimilated with the optimal interpolation scheme OI of DWD that provides the analysis for the operational global model GME. The SATEMS consist of profiles of temperature and humidity that are statistically derived by NOAA/NESDIS from the satellite radiances.

The new method applies a one dimensional variational analysis (1DVAR) in order to retrieve profiles that are assimilated at a second step in a similar way as the former SATEM data. Short term forecasts (3-hourly cycles) are used as background and first guess for the minimisation of 1DVAR.

During development of 1DVAR it was experienced that inconsistencies in vertical interpolations of the first guess profiles in OI and 1DVAR caused spurious biases. Being very small for one single assimilation step they accumulated to harmful sizes during several days. As a remedy only the analysis increments of 1DVAR (the differences to the first guess) are assimilated therefore and not the analysed values themselves.

Vertical background errors have been derived using the NMC-method with differences of 12 and 24 hourly forecasts valid for the same time. The sizes of background and observation errors have been tuned in order to provide best collocation of the 1DVAR retrievals compared to IFS analyses (Hess, 2005). As the top of the GME model is limited at 10 hPa, stratospheric fields are required for the radiative transfer simulation which is carried out using RTTOV-7. For that reason 12 to 33 hourly forecasts based on the previous 12 UTC analysis of IFS are received from ECMWF that are computed and arrive timely for the main forecasts runs at DWD. Bias correction is based on Eyre (1992) using scan angle and air mass correction, the latter with observed radiances of channels AMSU-A 4 and 9 as predictors.

Currently AMSU-A data of the satellites NOAA-15, NOAA-16 and AQUA are processed and assimilated. The use of NOAA-18 data is being prepared. Only temperature profiles are extracted for the time being, as the assimilation of humidity is deferred until HIRS and AMSU-B radiances are prepared for 1DVAR.

Figure 1 displays the observation coverage of a 3-hourly assimilation cycle. Data over land are removed during preprocessing, data with precipitation and sea ice are rejected during 1DVAR. The applied 1DVAR shows a significant improvement in forecast skill compared to the former use of SATEMS especially for the southern hemisphere where the data coverage of conventional observations is poor. Anomaly scores for 500 hPa geopotential height for a trial forecast run are given in Fig. 2.

Future plans are the assimilation of humidity and the assimilation of highly spectrally resolved infrared data from AIRS and IASI.

## References:

- Collard, A. *NWP SAF 1DVar User Manual*, NWP-SAF document, 2002
- Eyre, J. R. *A bias correction scheme for simulated TOVS brightness temperatures*, ECMWF Tech Memo, **176**, ECMWF, Reading, UK, 1992
- Hess, R. *Status of Assimilation Satellite Data at Deutscher Wetterdienst — tuning observation and background errors for 1D-Var* —, Proceedings of the 14th ITSC, pp. 740-746, Beijing, China, 25-31 May 2005
- Kelly, G. and P. Bauer, *The use of AMSU-A surface channels to obtain surface emissivity over land, snow and ice for Numerical Weather Prediction*, Proceedings of the 11th ITSC, pp. 167-179, Budapest, Hungary, 20-26 September 2000
- Parrish, D. F. and J. C. Derber, *The National Meteorological Center's Spectral Statistical Interpolation Analysis system*, Mon. Weather Rev., **120**, 1747-1763, 1992

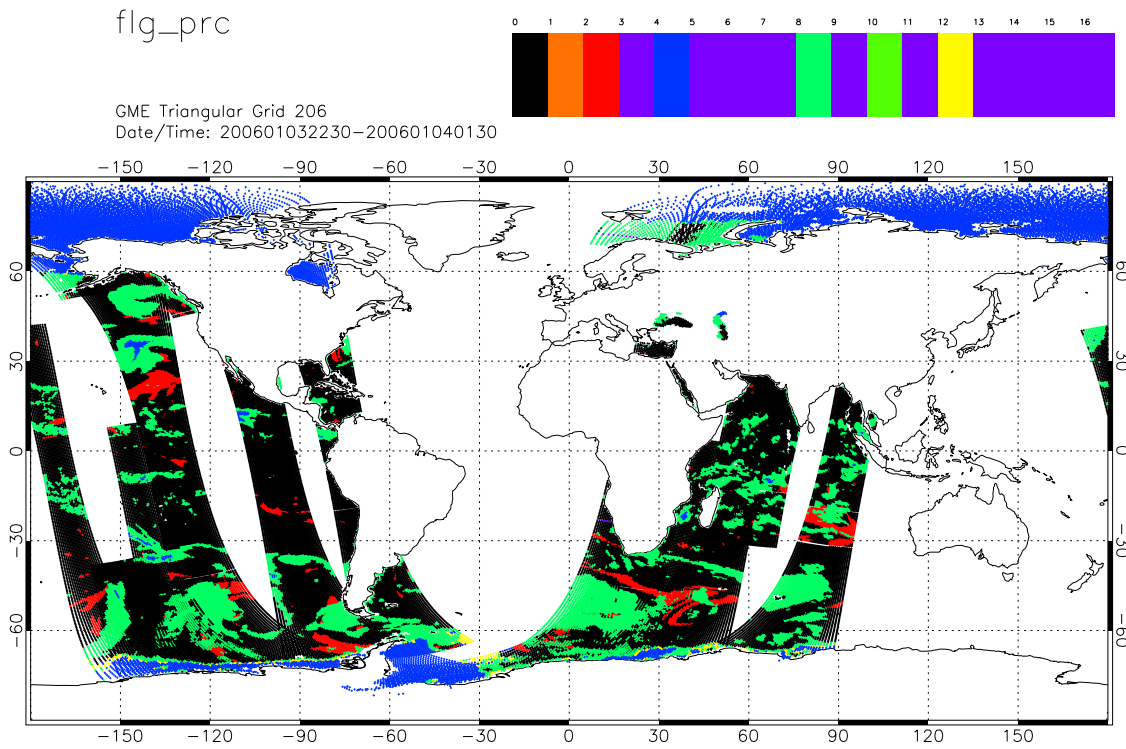


Figure 1: *Observation coverage of a 3-hourly assimilation cycle of satellites NOAA-15, NOAA-16 and AQUA. Displayed: processed data (black), rejected because of precipitation and of thick clouds (green), rejected because of sea ice (yellow and blue), rejected because minimisation of 1DVAR failed (red)*

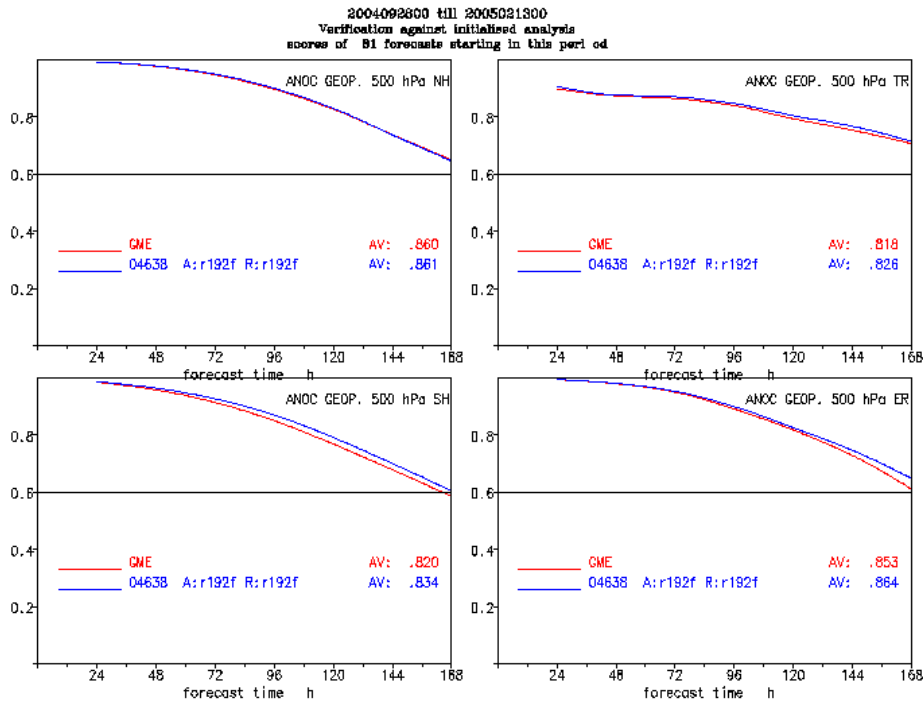


Figure 2: *Anomaly Scores for 500 hPa geopotential height for operational forecast with SATEMS (red) and trial run with 1DVAR (blue) for a trial period of 81 days. From left to right and top to bottom: northern hemisphere, tropics, southern hemisphere, Europe.*

# Doppler Radar Wind Data Assimilation with the JMA Meso 4D-VAR

Yoshihiro Ishikawa and Ko Koizumi  
Numerical Prediction Division, Japan Meteorological Agency  
1-3-4 Otemachi, Chiyoda-ku, Tokyo 100-8122, Japan  
E-mail: [ishikawa@met.kishou.go.jp](mailto:ishikawa@met.kishou.go.jp)

## 1. Introduction

The Japan Meteorological Agency (JMA) has been operating a mesoscale model (MSM) with a horizontal resolution of 10km to forecast mesoscale events over and around the Japan Islands since 2001. It is widely known that the accuracy of mesoscale numerical weather prediction (NWP), especially precise prediction of heavy rainfalls, is largely affected by the accuracy of the initial condition. Therefore, in order to improve the accuracy of initial state using various observations, JMA implemented a mesoscale four-dimensional variational assimilation system (Meso 4D-Var) in March 2002.

Eight airports in Japan are currently installed with operational Doppler radars (Fig. 1). These radars for safe aviation provide radial velocity data averaged in a 5km(radial direction) × 5.625 degrees(azimuthal interval) space up to the maximum detectable range 120km from each radar. The radial velocity data from six radars(except Chubu and Fukuoka) have been used in operation since March 2005 in the Meso 4D-Var. The ones from Chubu and Fukuoka have been used in operation since June 2005. At the moment, the Meso 4D-Var is used to assimilate the radial velocity data from eight radars (circles in Fig. 1) which are available at the analysis time.

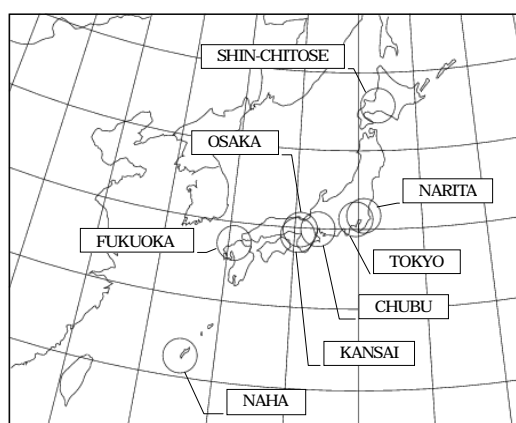


Fig. 1 Eight operational doppler radars and their maximum ranges in forecast domain of MSM.

## 2. Quality control and assimilation

First, in order to avoid the contribution of precipitation fall velocities to the Doppler velocities, data at the elevation angle larger than 5.9 degrees are not used. The data within 10km from a radar site are not used either because of back-scattering noise.

The provided radial velocity data are averaged values within a volume of 5km x 5.625 degrees with several information such as number of samples, standard deviation and max-min difference of wind speed within each volume. These additional informations are used for quality control. In the MSM routine, data are used only when following conditions are fulfilled.

- 1) the number of samples is above 10,
- 2) the standard deviation is below or equal to  $10 \text{ ms}^{-1}$ ,
- 3) the max-min difference is below or equal to  $10 \text{ ms}^{-1}$ ,
- 4) difference between observation and background value exceeds  $10 \text{ m s}^{-1}$ .

In addition to the above quality control, data within  $\pm 5 \text{ ms}^{-1}$  are removed due to the inappropriateness of land-echo removal procedure.

The data are thinned to about 20km apart horizontally after the quality control process. The observation operator for radial velocity is constructed as follows:

- 1)  $u$ - and  $v$ - component of wind of background field at each model level are interpolated to the observation point.
- 2) Since widened radar beam covers several layers of model domain, background  $u$  and  $v$  at the height of beam-center are calculated assuming that the beam intensity is a Gaussian function of distance from beam center. This method is slightly modified from the one employed in Seko et al. (2004).
- 3) Radial component is calculated from  $u$ - and  $v$ - component at the observation point.

### 3. Impact of radial velocity data

Three-hourly forecast-analysis cycle was performed without and with the radial velocity data in the following period 1-15 February and 1-13 September 2004. In each period, 18-hour forecasts were made four times a day at 00, 06, 12 and 18 UTC.

Figure 2 shows the radial velocity has positive impacts on precipitation forecasts. The improvement is found for moderate rain (10 mm / 3 hour, Fig. 2) but not so apparent for weak rain (not shown).

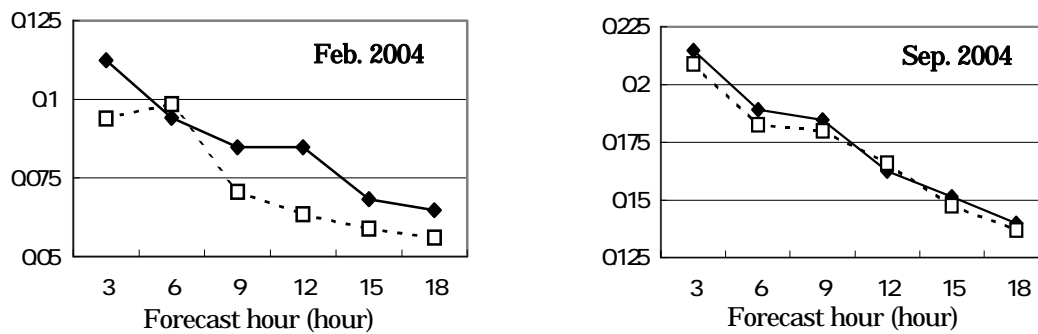


Fig.2 Threat score of precipitation forecast starting from analysis with radial velocity data (solid line) and without them (broken line). The threshold value is 10 mm per 3 hour. Left column is for the period from 1 to 15 Feb. 2004 and right column is for the period from 1 to 13 Sep. 2004.

Figure 3 shows a case of heavy rain in the experiment period. Figure 3a and 3c show, respectively, the forecast of 3-hour precipitation amount starting from the 4D-Var analysis without and with radial velocity ( $V_r$ ). Figure 3b shows the corresponding observation for Radar-AMeDAS from conventional weather radar.

Without Doppler radar data, the amount of the precipitation forecast in the center of forecast domain (indicated by circle) was much smaller than that of the observation. By assimilating  $V_r$  (Fig 3c), more precipitation is predicted and its precipitation pattern is closer to the radar observation.

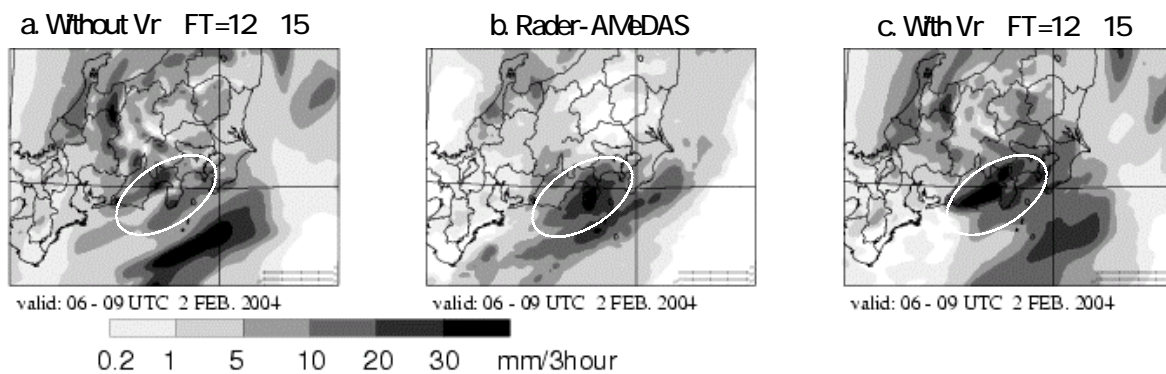


Fig.3 Forecast and observations of 3-hour precipitation amount at initial time of forecast is 18UTC 1 February 2004. Left: the forecast starting from the 4D-Var analysis without radial velocity ( $V_r$ ). Center: the Radar-AMeDAS observations. Right: the forecast starting from the 4D-Var analysis with  $V_r$ .

### Reference

Seko, H., T. Kawabata, T. Tsuyuki, H. Nakamura, K. Koizumi and T. Iwabuchi, 2004: Impacts of GPS-derived Water Vapor and Radial Wind Measured by Doppler Radar on Numerical Prediction of Precipitation, *J. Met. Soc. Japan*, **82**, 473-489.

# Assimilation Experiment of the Nerima Heavy Rainfall with a Cloud Resolving Nonhydrostatic 4 Dimensional Variational Data Assimilation System

Takuya KAWABATA<sup>a</sup>, Hiromu SEKO<sup>a</sup>, Tohru KURODA<sup>c</sup>, Kyuichiro TAMIYA<sup>a</sup>, Kazuo SAITO<sup>a</sup>, Tadashi TSUYUKI<sup>b</sup>

<sup>a</sup>Forecast Research Department of Meteorological Research Institute / JMA,

<sup>b</sup>Numerical Prediction Division of Japan Meteorological Agency

<sup>c</sup>Meteorological Research Institute / JST Cooperative System for Supporting priority Research

## 1. Introduction

The Forecast Research Department of the Meteorological Research Institute (MRI) has been developing a high-resolution nonhydrostatic 4 dimensional variational assimilation system (NHM-4DVAR) based on the Japan Meteorological Agency nonhydrostatic model (JMA-NHM) since April 2002 in the collaboration with the Numerical Prediction Division of JMA. The aim is to apply a 4DVAR technique to the mesoscale convective cloud system with a cloud resolving resolution less than 2 km. Since the 4DVAR gives the optimized 3 dimensional field between the model dynamics and the observation, it seems that 4DVAR provides numerical models more suitable initial conditions to simulate the convective system if observed data are well utilized.

We applied the NHM-4DVAR to the Nerima heavy rainfall event occurred at 21 July 1999. Seko et al. (2005) applied the JMA hydrostatic Meso 3DVAR and NHM-3DVAR to this event and reproduced associated heavy rainfall, but a statistical relation between the relative humidity and updraft velocity was introduced. In this report, assimilating observed data with NHM-4DVAR, deep convection under the weak environmental forcing associated with the heavy rainfall is successfully reproduced.

## 2. NHM-4DVAR

The tangent linear model and the adjoint model of NHM-4DVAR are based on the year 2002 version of JMA-NHM. A prototype version for dry dynamics was initially developed (Honda et al., 2003). Advection term of water vapor is included (Kawabata et al., 2004), and the perturbations of the lateral boundary conditions are also newly considered, associated with the control variables.

A set of control variables is designed for high resolution 4DVAR. Horizontal wind ( $u$ ,  $v$ ), vertical wind ( $w$ ), nonhydrostatic pressure, potential temperature, surface pressure and pseudo relative humidity (Dee and Da Silva, 2002) were chosen. We do not consider any balance mode of control variables except for the hydrostatic pressure, because it is difficult to define balance mode in high resolution such as 2 km and short time scale.

The Radial Wind data derived by the Doppler radars (RW), the GPS Precipitable Water Vapor (PWV) data and the surface observation data are available as the high temporal and spatial resolution data (Kawabata et al., 2005).

## 3. Assimilation experiment

NHM-4DVAR with a horizontal resolution of 2 km is applied to the assimilation experiment. The assimilation window is from 0500 UTC to 0600 UTC, 21 July 1999 which includes the generation time of the Nerima cells but excludes their mature stage. The forward model is a full-scale JMA-NHM which includes 5 category cloud microphysical processes, while the adjoint model is a simplified model. The horizontal domain is 240 km x 240 km which covers the Kanto plain. In NHM-4DVAR, RW data are assimilated with 1 minute interval by every elevation angle and the RW data from 0.7 to 5.4 degree elevation angle are used for assimilation to remove undesirable high elevation angle data. GPS-PWV data are assimilated with 5 minutes interval, and the surface wind and temperature data observed by the Automated Meteorological Data Acquisition System (AMeDAS) of JMA are assimilated with 10 minutes interval. After the assimilation, we performed a 3 hour forecast with the assimilated initial field.

The time sequence of the cost function  $J$  with respect to iteration numbers is shown in Fig. 1. Total value of  $J$  becomes half and decreases with a log scale. Most part of this decrease is by the decrease of the cost of RW data. Because the costs of GPS-PWV data and the surface observation

are minimized well and the orders of each cost function value are same orders of the number of each observations, the minimization process successfully converged.

Figure 2a shows composite rainfall amount observed by radar corrected by AMeDAS rain gage data. A heavy rainfall area over 100 mm/hour exists around Nerima. But in the first guess field (Fig. 2c), any strong rainfall area does not exist. On the other hand, in the forecast field (Fig. 2b), location and intensity of the Nerima cells were well reproduced, and other convective areas were also reproduced except for their intensities. Figure 3 shows the time sequence of rainfall amount in every 10 minutes observed by rain gage of AMeDAS at Nerima and the forecast at a model grid point near Nerima cells. Both rainfall amounts are about 15 mm to 25 mm between 0630 UTC and 0710 UTC and their time sequence are quantitatively in good agreement. These facts show that the lifetime and the intensity of Nerima cells were well reproduced.

### References

1. Dee, Dick P., Arlindo M. Da Silva, "The Choice of Variable for Atmospheric Moisture Analysis", Monthly Weather Review, 155-171, 2003
2. Honda, Y., T. Kawabata, K. Tamiya, K. Aonashi, T. Tsuyuki and K. Koizumi, "Development of a 4DVAR data assimilation system ad JMA"(in Japanese), Preprints. 5th Workshop on the Nonhydrostatic Model, 2003
3. Kawabata, T., T. Kuroda, Y. Honda, K. Tamiya, K. Aonashi, T. Tsuyuki, and K. Koizumi, "A 4DVAR data assimilation system for the JMA Nonhydrostatic model to assimilate water vapor data" (in Japanese), Preprints. Spring meeting of Meteorological Society of Japan, 2004
4. Kawabata, T, H. Seko, T. Kuroda, Y. Wakatsuki, Y. Honda, K. Tamiya, K. Aonashi, Y. Shoji, K. Saito, T. Tsuyuki, "A cloud resolving 4DVAR data assimilation system based on the JMA non-hydrostatic model", CAS/JSC WGNE Res.Act. Atmos. Ocea. Modelling, 01-19 01-20, 2005
5. Seko, H, T. Kawabata, T. Tsuyuki, "Data Assimilation Experiments of Nerima Heavy Rainfall", CAS/JSC WGNE Res.Act. Atmos. Ocea. Modelling, 01-41 01-42, 2005

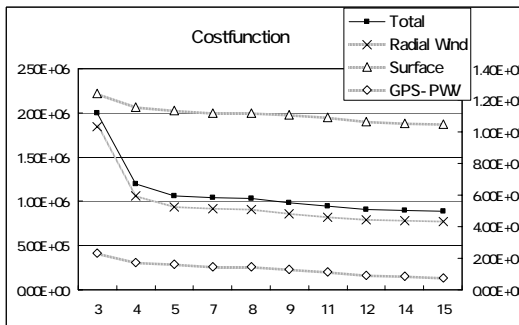


Fig. 1. Time sequence of the value of the cost function J. 'Total' and 'RW' use the left Y-axis and 'Surface' and 'GPS-PWV' use the right Y-axis.

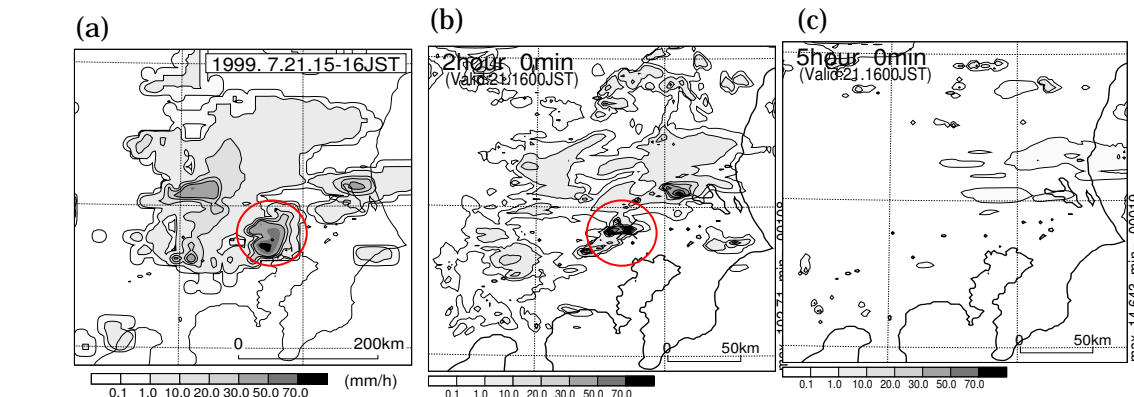


Fig.2. 1 hour accumulated rainfall amount from 0500 UTC to 0600 UTC. (a) is Radar-AMeDAS analysis, (b) is forecast result and (c) is the first guess field. Red circles show the Nerima cells.

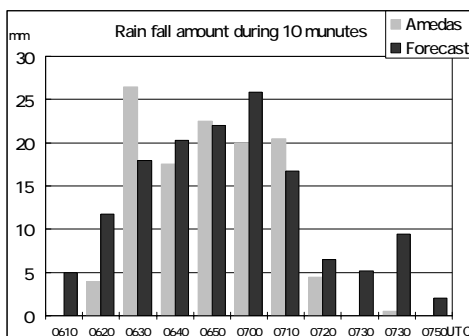


Fig. 3. Time sequence of rainfall amount in every 10 minutes. Gray bars show observation at Nerima. Black bars show forecasting result at the developing point of Nerima heavy rainfall.

## Assimilation of Radar Data in the Mesoscale NWP-Model of DWD

Stefan Klink, Klaus Stephan, Christoph Schraff

Deutscher Wetterdienst, Kaiserleistr. 29/35, 63067 Offenbach am Main, Germany

e-mail: stefan.klink@dwd.de, klaus.stephan@dwd.de, christoph.schraff@dwd.de

The main focus of LMK (Doms and Förstner, 2004), which is being developed as a meso- $\gamma$ -scale version of the operational non-hydrostatic limited area model LM, is on the very short range prediction of severe weather, which often forms in context with deep moist convection. Thus, in addition to the assimilation of conventional data, as a first step 2D radar reflectivity derived from the German radar network will be introduced in the nudging-type analysis of LMK. Using the Latent Heat Nudging (LHN) technique (Jones and Macpherson 1997; Macpherson 2001) the latent heating of the atmospheric model is scaled by the fraction  $a$  of observed to modelled precipitation in order to drive the modelled rain rates towards observed ones.

Past experiments with a purely diagnostic precipitation scheme have shown that precipitation patterns can be assimilated in good agreement with those observed by radar, both in position and amplitude. In order to simulate the horizontal distribution of precipitation in mountainous terrain more realistically, a prognostic treatment of precipitation (Gassmann 2002; Baldauf and Schulz 2004) including advection has been introduced in the model, and is used operationally in the LME (LM Europe). It tends to decorrelate the surface precipitation rate from the vertically integrated latent heat release and thereby violate the basic assumption to the Latent Heat Nudging (LHN) approach. This, and resulting problems have been shown by Klink and Stephan (2005), and they also suggested possible adaptations to the LHN scheme.

At horizontal model resolutions of 3 km or less, the prognostic treatment of precipitation allows the model to distinguish between updrafts and downdrafts inside deep convective systems. Compared to using the diagnostic precipitation scheme, it modifies both the 3-D spatial structure and the timing of the latent heating with respect to surface precipitation. Therefore, three revisions have been introduced to the LHN scheme. Two of them addressing spatial aspects and a third one an important temporal issue:

- In updraft regions at the leading edge of convective cells, very high values of latent heat release occur often where modelled precipitation rates are low. Thus high values of the scaling factor  $a$  and of the latent heat nudging temperature increments often occur. To mitigate this, the upper limit for  $a$  is reduced to 2 and the lower limit increased accordingly to 0.5. This adaptation reduces the simulated precipitation amounts during the LHN.
- In downdraft regions further upstream in convective cells, high precipitation rates occur often where latent heating is weak or even negative in most vertical layers. In order to avoid negative LHN temperature increments and cooling where the precipitation rate should be increased (and vice versa), only the vertical model layers with positive simulated latent heating are used to compute and insert the LHN increments. This modification tends to render the increments more coherent and the scheme more efficient.
- Precipitation produced by the prognostic scheme will take some time to reach the ground where it is compared to the radar-derived surface precipitation rate. Thus, the conventional LHN scheme can notice only with some temporal delay when it has already initiated precipitation aloft. Therefore, an immediate information on the precipitation rate already initialised is required, i.e. a sort of undelayed 'reference precipitation'  $RR_{ref}$  which is used merely to replace the delayed prognostic model precipitation  $RR_{mo}$  in the computation of the scaling factor  $a$ . One choice is found to be the vertically averaged precipitation flux.

The above mentioned revisions have been tested for an 11-day convective summer period from 7 to 18 July 2004. An assimilation cycle and 3 daily forecast runs from 00, 12, and 18 UTC have been carried out with the LMK configurations for the general model setup ( $\Delta x = 2.8$  km, 50 vertical layers). In addition to the major revisions, several minor modifications have been implemented in the LHN scheme (e.g. at the grid point search), and the LHN configuration in the experiments also included the following features:

- use of a radar composite, based on the so-called precipitation scans of the 16 German radar sites, every 5 minutes, and application of a blacklist to reject suspicious radar pixels (e.g. near wind power plants)

- limitation of LHN to grid points with  $RR_{obs} > 0.1$  mm/h or  $RR_{ref} > 0.1$  mm/h
- search for nearby profiles of latent heat release, if both  $RR_{ref}$  and the latent heating are 'too small'; use of an idealised 'climatological' profile in case of unsuccessful search
- vertical filtering of temperature increments
- adjustment of specific humidity (by preserving relative humidity, and by nudging towards saturation at cloud-free model grid points with observed precipitation)

The LHN experiment is evaluated in comparison to a control experiment without LHN (see also Schraff et al. 2006). Figure 1 shows statistical scores for the whole period. The frequency bias (FBI) indicates that during the assimilation, precipitation is greatly underestimated at daytime without LHN, and it is increased significantly by LHN (see figure 1c). While the areal extent (threshold: 0.2 mm) is matched very well with LHN, rain amounts are overestimated by about 50% for the 2-mm threshold (not shown), but less strongly than in previous experiments that used the old LHN scheme. Moreover, LHN greatly improves the location of the precipitation patterns during the assimilation (see fig. 1a). This positive impact of radar data is visible in the 18-UTC forecasts for up to 6 hours (fig. 1b) on average. In the 0-UTC and 12-UTC forecasts, however, the benefit from LHN decreases rapidly within 2-3 hours. Whether this rapid decrease is partly due to the double penalty problem inherent to local grid point verification of high resolution models still needs to be evaluated. In general the limited forecast impact is similar to results gathered by others, using different assimilation methods for radar data.

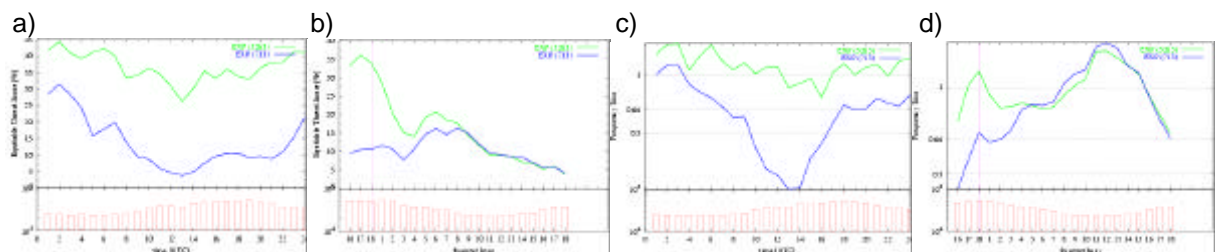


Figure 1: Mean equitable threat scores (ETS) for hourly precipitation during the assimilation cycle as a function of daytime (a) and for hourly precipitation during 18 UTC forecasts as a function of forecast time (b) and mean frequency biases (FBI) for assimilation (c) and for 18 UTC forecasts (d) for a threshold of 0.2 mm. These mean scores were obtained by averaging over a 10 day period. Assimilation cycles: nudging without LHN (blue, label "EXP(713)") and nudging with LHN (green, label "EXP(5263)"). The vertical purple lines in (b) and (d) indicate the starting time of the free forecasts.

To conclude, several adaptations to the LHN scheme have been found which enable the model with prognostic precipitation to simulate the rain patterns in good agreement with radar observations during the assimilation. The overestimation of precipitation is reduced significantly compared to previous LHN versions. Thus, the problems related to prognostic precipitation appear to be mitigated to a satisfactory degree. However, the scheme still needs to be tested for stratiform precipitation, and the rapid decrease of benefit in the forecasts remains a shortcoming.

#### References:

- Baldauf, M., and J.-P. Schulz: Prognostic Precipitation in the Lokal Modell (LM) of DWD. *COSMO Newsletter*, No. 4, 177-180 (available at [www.cosmo-model.org](http://www.cosmo-model.org)), 2004.
- Doms, G., and J. Förstner: Development of a Kilometer-Scale NWP-System: LMK. *COSMO Newsletter*, No. 4, 159-167 (available at [www.cosmo-model.org](http://www.cosmo-model.org)), 2004.
- Gassmann, A.: 3D-transport of Precipitation. *COSMO Newsletter*, No. 2, 113-117 (available at [www.cosmo-model.org](http://www.cosmo-model.org)), 2002.
- Jones, C. D., and B. Macpherson: A Latent Heat Nudging Scheme for the Assimilation of Precipitation Data into an Operational Mesoscale Model. *Meteorol. Appl.*, 4, 269-277, 1997.
- Klink, S., and K. Stephan: Latent heat nudging and prognostic precipitation. *COSMO Newsletter*, No. 5, 124-131 (available at [www.cosmo-model.org](http://www.cosmo-model.org)), 2004.
- Macpherson, B.: Operational Experience with Assimilation of Rainfall Data in the MetOffice Mesoscale Model. *Meteorol. Atmos. Phys.*, 76, 3-8, 2001.
- Schraff, C., K. Stephan, and S. Klink: Revised Latent Heat Nudging to cope with prognostic precipitation. *COSMO Newsletter*, No. 6, (available at [www.cosmo-model.org](http://www.cosmo-model.org) in early 2006).

# Influence of Typhoon Bogus Parameters on the Typhoon Forecasts

Masaru Kunii

Meteorological Research Institute, Tukuba, Japan

## 1. introduction

It is important to produce the accurate initial fields to improve the forecast of typhoons. Due to the lack of adequate observational data near the typhoon center, the typhoon bogus data, which is produced empirically, has been used in producing initial fields by the 4-dimensional variational data assimilation (4DVAR) system for meso-scale model (MSM) of the Japan Meteorological Agency (JMA). However, there is some arbitrariness in setting the bogus parameters such as the arrangement and the observational errors and those parameters don't depend on the first guess from which the bogus profile is calculated, so the usage of the bogus data is not considered as optimal in the current assimilation system.

In this paper, grasping the property of bogus data, the sensitivity experiments on the effects of the density and observational error of them are carried out.

## 2. Experiment design

Under the present circumstances, the bogus data are arranged as concentric circles with an interval of 200km in radius, and their observational errors are set at the same level of in-situ observations like radio sonde. In order to evaluate the sensitivity of bogus parameters with 4DVAR system, a series of experiments are executed (Table 1). The target is Typhoon MA-ON (2004), and the assimilation period is 3-hour from 09UTC 8 October 2004. The typhoon bogus data are assimilated as the observational data at 12UTC.

**Table 1** The index of experiments

Exp	Error Ratio	Density Ratio	Level
CNTL	None	None	All
TYB	1	1	All
ERROR1/2	0.5	1	All
ERROR2	2	1	All
DENS2	1	2	All
DENS1/2	1	1/2	All
ERROR1/2U	0.5	1	Under 600hPa

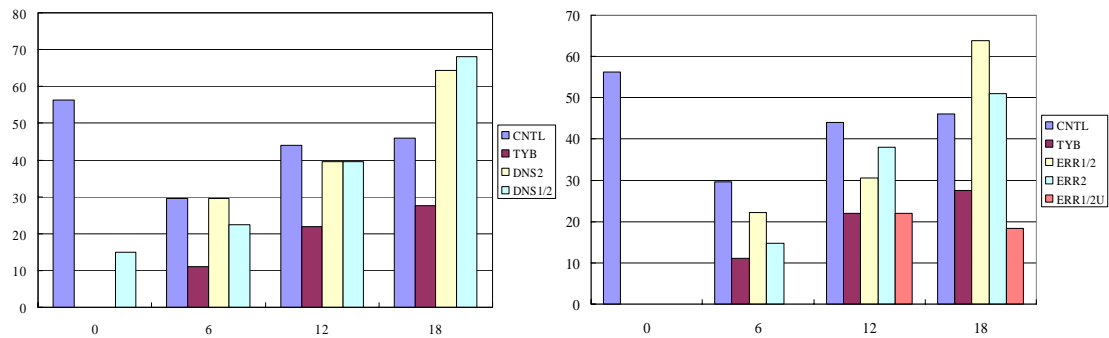
## 3. Influence of bogus parameters

Figure 1 shows the averaged errors of forecasted typhoon tracks from all experiments. The

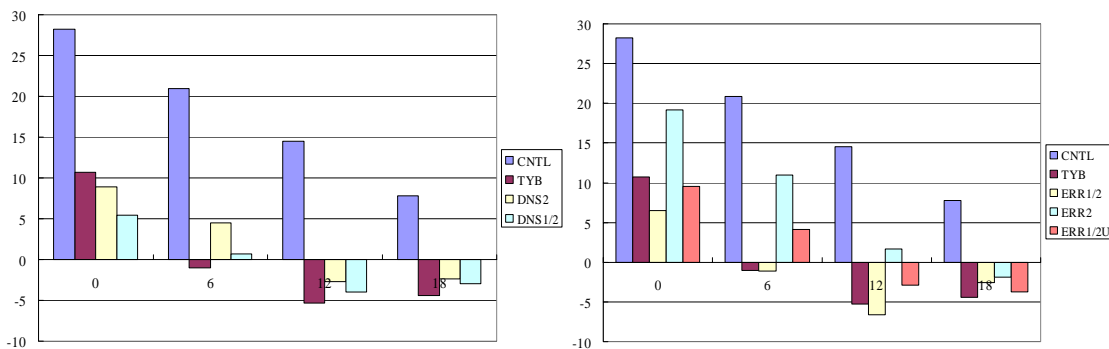
result of DNS2 and DNS1/2 were much worth than CNTL, without bogus. In DNS2 experiment, error correlation among bogus data can't be ignored because of relatively short distance between them. Conversely DNS1/2 was not enough to modify the initial fields. The experiments ERR1/2 and ERR2 were also worse than CNTL at the later stage of forecast period, but ERROR1/2U improved the forecast over TYB.

Figure 2 shows the averaged errors of forecasted typhoon central sea-level pressure from all experiments. The results from the experiments DNS2, DNS1/2, ERR1/2 and ERR2 got better or neutral, but that of ERR2 got worse.

The results suggest that the typhoon forecasts are sensitive to initial fields and that the typhoon bogus is effective for producing analysis fields only when the bogus parameters are specified appropriately.



**Fig.1** The errors of forecasted typhoon tracks at every 6 hours from 12UTC 8 October 2004. X-axis represents forecast time and y-axis represent typhoon track error.



**Fig.2** The errors of forecasted typhoon central sea-level pressure at every 6 hours from 12UTC 8 October 2004. X-axis represents forecast time and y-axis represents the error of typhoon central sea-level pressure.

---

Corresponding author address : Masaru KUNII, Meteorological Research Institute, 1-1 Namigane Tukuba Ibaraki 305-0052, Japan email : [mkunii@mri-jma.go.jp](mailto:mkunii@mri-jma.go.jp)

# Local ensemble transform Kalman filtering with an AGCM at a T159/L48 resolution

Takemasa Miyoshi\*<sup>†</sup> and Shozo Yamane\*\*

\*Numerical Prediction Division, Japan Meteorological Agency

\*\*Chiba Institute of Science

In August 2005, we began to develop the local ensemble transform Kalman filter (LETKF, Hunt 2005) with AFES (AGCM for the Earth Simulator, Ohfuchi et al. 2004) at a T159 horizontal and 48-level vertical resolution in collaboration among the Numerical Prediction Division, Japan Meteorological Agency (NPD/JMA), the Chiba Institute of Science, and the Earth Simulator Center (ESC). We developed the LETKF system based on the system constructed by Miyoshi (2005) at the University of Maryland where originally LETKF has been invented.

A main limitation of ensemble Kalman filter (EnKF) experiments published thus far is the lower resolutions than the currently operational data assimilation or ensemble prediction systems (EPS). The experimental resolutions are at most as large as T62, whereas operational EPS have at least as large as a T106 resolution. A higher resolution model uses more precise physical processes and resolves smaller scale phenomena, possibly introducing larger substantial degrees of freedom of the dynamical error structures. This causes the increase of required ensemble size for stable EnKF, an important disadvantage. This research tackles the limitation by applying LETKF to the T159 AFES model, corresponding grid size of 480x240x48, a similar resolution to operational systems.

Generally EnKF has two parameters: the covariance inflation parameter and covariance localization scale parameter. The former parameter is objectively estimated as in Miyoshi (2005) following a suggestion by Kalnay (pers. comm.). LETKF requires two types of localization parameters: the local patch size and observational localization scale. In LETKF, it is better that we choose local patch size sufficiently larger than the observational localization scale, although larger local patch size requires more computations. We assume horizontal isotropy, but vertically we define different localization parameters. We choose 11x11x5 local patch and 2.0-grid horizontal and 1.0-grid vertical observational localizations in the following experiments.

We follow observing systems simulation experiment (OSSE) methodology in a perfect model scenario, where we generate the true nature run by a long-term integration of the same T159/L48 AFES model and sample observations from it. We take observations every 6 hours in the time domain and in the spatial domain regularly one at every 5x5x4 grid points, just 1% of the entire grid points. The observed variables are the zonal and meridional wind components, temperature, specific humidity, and surface pressure with error standard deviations of 1.0 m/s, 1.0 K, 0.1 g/kg, and 1.0 hPa, respectively. The initial ensemble members to initiate the data assimilation cycle are randomly chosen from a nature run in a similar season, the initial ensemble mean is an analogue of the climatological mean.

Fig. 1 shows time series of the analysis root mean square errors (RMSE) of the surface pressure for 30 days. It is noted that even with 10 members, LETKF seems stable, at least it is not diverging. Increasing ensemble size, we see LETKF be more stable with lower error levels, about half as large as the observational error level. Fig. 2 shows the sensitivity to the ensemble size. At the first assimilation step, we see linear decrease of the analysis errors up to about 80 members. Increasing the ensemble size beyond 320 does not show significant change of the analysis error levels, which is consistent with the fact that the substantial degrees of freedom in the local patch are around 400. After 10-day data assimilation cycles, the error decreasing trend is slower than linear, the difference between 40 and 80 members becomes smaller.

Table 1 shows timing results of one-step LETKF computations without forecast computations. If we use as many computational nodes as the ensemble size and they are less than 80, it takes just less than 4 minutes on the Earth Simulator, peak performance of 64 GFlops per node. The parallel efficiency increases with ensemble size, about 99.99% parallelization ratio with more than 80 members.

---

<sup>†</sup> Corresponding author address: Numerical Prediction Division, Japan Meteorological Agency, 1-3-4 Ote-machi, Chiyoda-ku, Tokyo 100-8122, Japan. E-mail: miyoshi@naps.kishou.go.jp

In summary, we developed and tested LETKF with the T159/L48 AFES model and found that even with the resolution as high as operational EPS, ensemble size of the order of less than 100 shows quite stable and good filter performance. The computational time is also applicable for operations, we are now at a stage of developing realistic observational operators and assimilating real observations.

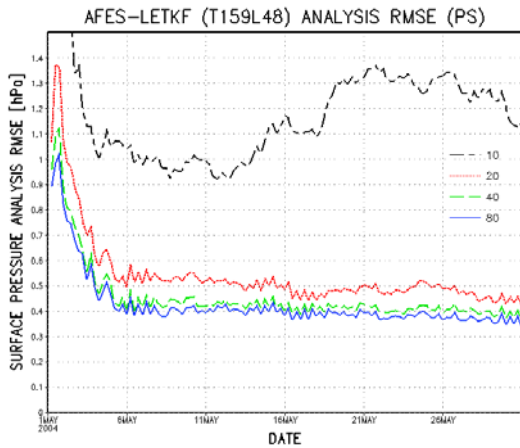


Figure 1. Time series of the analysis errors of LETKF for 30 days with 10 (black long-short-dashed line), 20 (red broken line), 40 (green dashed line), and 80 (blue solid line) ensemble members. The errors are measured by the RMSE of the surface pressure.

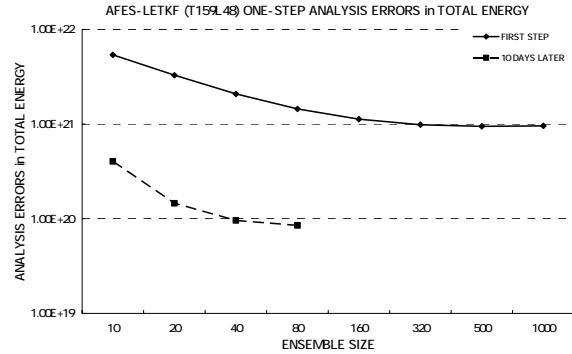


Figure 2. Analysis errors in the total energy norm at one-step analyses of LETKF with changing the ensemble size. Solid and dashed lines show the analyses at the first-step and 10 days later from the first-step, respectively.

Table 1 Timing (sec.) of LETKF on the Earth Simulator

Ensemble size	5 nodes	10 nodes	20 nodes	40 nodes	80 nodes	160 nodes	200 nodes	240 nodes
10	382	195	115	67	47			
20	714	360	197	107	66			
40	1389	708	360	189	112			
80		1583	824	413	220			
160				1205	626	336		
320						1139		
500							2270	1924
1000							10595	

## Acknowledgements

We thank members of the chaos/weather group of the University of Maryland, especially Prof. Eugenia Kalnay for fruitful discussions. We also thank Drs. Wataru Ohfuchi and Takeshi Enomoto of ESC, and Yoshiaki Takeuchi and Ko Koizumi of NPD/JMA for kind understanding and support for this project. Most computations of this research have been performed on the Earth Simulator.

## References

- Hunt, B. R., 2005: Efficient Data Assimilation for Spatiotemporal Chaos: a Local Ensemble Transform Kalman Filter. arXiv:physics/0511236v1, 25pp.
- Miyoshi, T., 2005: Ensemble Kalman filter experiments with a primitive-equation global model. Ph.D. dissertation, University of Maryland, 197pp.
- Ohfuchi, W., H. Nakamura, M. K. Yoshioka, T. Enomoto, K. Takaya, X. Peng, S. Yamane, T. Nishimura, Y. Kurihara, and K. Ninomiya, 2004: 10-km mesh meso-scale resolving simulations of the global atmosphere on the Earth Simulator: Preliminary outcomes of AFES (AGCM for the Earth Simulator). *J. Earth Simulator*, **1**, 8–34.

## High resolution model simulation of a Nor'wester over Kolkata, India

P. Mukhopadhyay<sup>1</sup> and H. A. K. Singh<sup>2</sup>

<sup>1</sup>Forecasting Research Division, Indian Institute of Tropical Meteorology,  
Dr. Homi Bhabha Road, Pune-411008, INDIA (mpartha@tropmet.res.in)

<sup>2</sup> India Meteorological Department, Doppler Weather Radar, 1, K. S. Roy Road  
Kolkata-700001, INDIA

### 1. Introduction

Eastern and north-eastern states of India experience thunderstorms with high frequency during pre-monsoon (March-May) season. The thunderstorms are locally known as “Nor’wester” as it travels from northwest to southeast direction. These storms are generally associated with strong wind followed by heavy rain and sometimes with hail. Due to smaller spatial and temporal dimension, Nor’westers are generally not resolved by conventional synoptic observational network. It remains a challenge of numerical weather prediction to simulate such system using a model. As such an attempt is made to simulate the nor’wester of 22 May 2003. This happened to be the last nor’wester of premonsoon season of 2003 and it caused havoc to the city of Kolkata and its surrounding areas.

### 2. Model and Methodology

RAMS version 4.30 is used to carry out the simulation experiments. RAMS is used with two way interactive nested grids of resolutions 16 km and 4 km as shown in Fig. 1. The grids are centered at 22.6° N, 88.4° E and the number of grid points for 16 km resolution is 68 x 68 in east-west and north-south direction and that for 4 km grid are 58 x 58. The numbers of terrain following levels in both the domains are 36. A Modified Kuo convection scheme (Tremback, 1990) is used for the large scale precipitation and Bulk microphysics of Walko et al. (1995) is used for prognosing cloud constituents and grid scale precipitation. A two-stream radiation scheme developed by Harrington (1997) is used. Two simulation experiments are carried out to study the impact of assimilating regional data on the simulation. In one of the experiments (expt-A) RAMS is initialized with 0000 UTC NCEP/NCAR reanalyses data (2.5 deg x 2.5 deg) of 22 May 2003 and run in four dimensional data assimilation (FDDA) nudging mode for initial six hours and then followed by 12 hour integration in forecast mode till 1800 UTC of 22 May. In the other experiment (expt-B), the radiosonde data at 0000 UTC of 22 May from the stations namely Kolkata, Ranchi and Patna (located in the Gangetic plains at a distance of ~250-300 km) are assimilated in the gridded analyses and the model is run in similar manner as that of expt-A.

### 3. Discussion of results

Simulation experiments suggest that the incorporation of the upper air and surface data have significantly improved the initial condition in terms of better representation of the thermodynamic instability prevailing over the region. Different thermodynamic instability indices derived from the enhanced input is found to be closely matching with the values derived from the radiosonde data of the stations (Kolkata, Ranchi and Patna). Mainly due to this improvement the 12 hour forecast by expt-B has significantly improved in comparison to that of expt-A. The streamline analyses at 850 hPa of 0000 UTC of 22 May with NCEP (Fig. 2a) and enhanced NCEP data (Fig. 2b) show significant change. The streamline in Fig. 2b suggests a cyclonic circulation over Bihar region which is weakly seen at the north-west corner of the coarse domain in Fig. 2a. The corresponding analyses for the relative humidity (Fig. not shown) at 850 hPa show particularly over Bihar region isolines of 60-90% in the enhanced analyses. The assimilation of regional upper air data appears to have improved the instability over the said region. The forecast wind barbs in expt-A are able to show a circulation (Fig. not shown) at 6 hour forecast (1200 UTC) and wind speed of the order of 15 Kt is predicted over Kolkata which matches well with the Doppler observation. At 7, 8 and 9 h (1300, 1400 and 1500 UTC) forecasts, the wind over Kolkata is found to be of north-westerly and of the order of 20-25 knot

which is better comparable with the Doppler radar derived wind of the corresponding hour than that of expt-B. The hourly forecast of cloud condensate at 850 hPa is also significantly improved in terms of location and strength in expt-B (Fig. 3) as supported by the LWC of Doppler radar shown in Fig. 4 as compared to that of expt-B. The 12 hour accumulated precipitation by expt-A and B are shown in Fig. 5a and 5b and compared with the CPC 24 hour accumulated and Doppler radar 12 hour accumulated precipitation (Fig. 5c and Fig. 5d). Expt-A has shown significant improvement in improving the precipitation (Fig. 5b) which is found to be in and around Kolkata and well supported by the Doppler estimate (Fig. 5c). However the amount of forecast precipitation (2 cm) by expt-A is found to have underestimated the observed value of 7-8 cm.

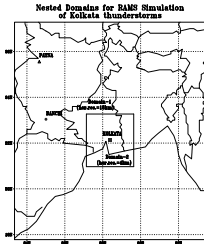


FIG. 1. Domain of the two grids along with the locations of three upper air stations. Grid-1 stands for 16 km and Grid-2 stands for 4 km domain.

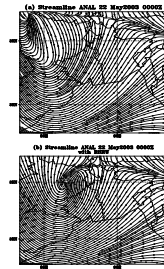


FIG. 2. Streamline analysis at 850 hPa of 22 May 2003 (a) NCEP interpolated to RAMS 16-km grid; (b) enhanced analysis at 0000 UTC.

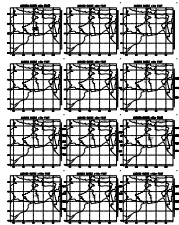


FIG. 3. Hourly forecast of total cloud condensate ( $\text{g kg}^{-1}$ ) at 850 hPa by coarse domain as obtained from EXP-3 for 22 May 2003 Nor'wester.

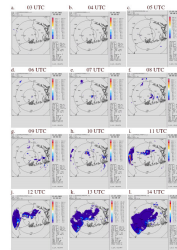


FIG. 4. Doppler radar estimated hourly cloud liquid water content of 12 March 2003 Nor'wester.

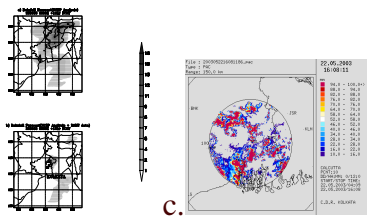


Fig. 5 Precipitation forecast (a) 12-h accumulated in expt-A; (b) 12-h accumulated in expt-B; and (c) Doppler radar 12-h accumulated estimate.

## References

- Klemp, J. B., and R. B. Wilhelmson, 1978a: "The simulation of three-dimensional convective storm dynamics". J. Atmos. Sci., **35**, 1070-1096.
- Davies, H. C., 1983: "Limitations of some common lateral boundary schemes used in regional NWP models". Mon. Wea. Rev., **111**, 1002-1012.
- Tremback, C. J., 1990: "Numerical simulation of a mesoscale convective complex: Model development and numerical results". PhD dissertation, Atmos. Sci. Paper No 465, Colorado State University, Department of Atmospheric Science, Fort Collins, CO 80523.
- Harrington, J. Y. 1997: "The effects of radiative and micro-physical processes on simulated warm and transition season Arctic stratus". PhD Dissertation, Atmospheric Science Paper No 637, Colorado State University, Department of Atmospheric Science, Fort Collins, CO 80523, 289 pp.
- Walko, R. L., W. R., Cotton, M. P., Meyers, and J. Y., Harrington, 1995: "New RAMS cloud microphysics parameterization Part I: the single-moment scheme". Atmos. Res., **38**, 29-62.

# Changing the resolution of the inner loop of global 4D-Var at JMA

A.Narui

*Numerical Prediction Division, Japan Meteorological Agency  
1-3-4 Otemachi, Chiyoda-ku, Tokyo 100-8122, JAPAN  
narui@met.kishou.go.jp*

## 1. Introduction

The four-dimensional variational data assimilation (4D-Var) was introduced into the JMA Global Spectral Model since February 2005. The incremental method (Coutier et al. 1994) is used for 4D-Var, and the resolutions of the outer and inner loops are TL319 and T63 respectively. Although T63 may be too rough for relatively small scale phenomena, especially for the analysis of typhoon, higher resolutions are not available due to the limitation of computer resources. As we are going to introduce a new computer system in 2006, which enable us to use a higher resolution inner loop for 4D-Var, we have developed 4D-Var of the higher resolution inner loop (T106) and examined its impact on the global model forecasts.

## 2. Parallel experiments

Parallel run tests to compare the performance of 4D-Var of T106 inner loop (Test) and that of T63 inner loop (Cntl) were conducted for each one-month period, August 2004 and January 2005. The model is Global Spectral Model and the resolution is TL319. The 216-hour forecasts were conducted from 12UTC for each day from 1<sup>st</sup> to 21<sup>st</sup> August and from 1<sup>st</sup> to 21<sup>st</sup> January and anomaly correlation was calculated from these 21 forecasts for each period.

Figure 1 is the comparison of the RMSE between the radio-sonde observation and the analysis fields at standard pressure levels for the experiment of August 2004. The RMSE of Test (red line) is smaller than Cntl (blue line) for both of temperature and zonal wind. It means the analysis field from the higher resolution inner loop is nearer to the observation.

Figure 2 is the comparison of the anomaly correlation of 500hPa height forecasts in the Northern Hemisphere between Test (red line) and Cntl (blue line) for August 2004 and January 2005. The anomaly correlation of Test is better than that of Cntl. Similar results were also obtained for almost all elements for all regions.

The T106 inner loop will be operational in March 2006.

## 3. References

Coutier, P., J.-N. Thepaut, and A. Hollingsworth, 1994: A strategy for operational implementation of 4D-Var, using an incremental approach. *Quart. J. Roy. Meteor. Soc.*, 120, 1367-1387.

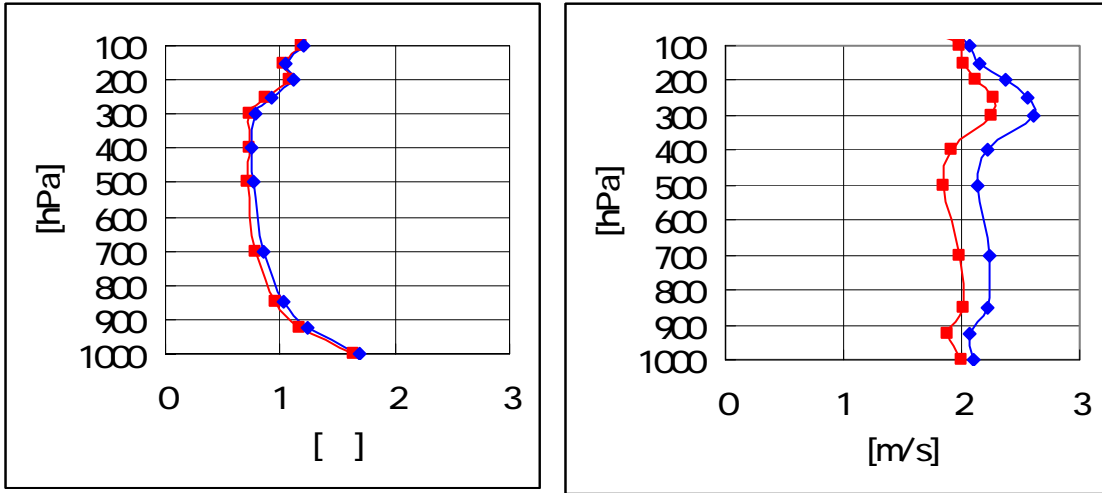


Fig.1 The comparison of the RMSE between the radio-sonde observation and the analysis fields at standard pressure levels for the experiment of August 2004. The left and right figures are for temperature and zonal wind respectively. The red line means Test and the blue line indicates Cntl.

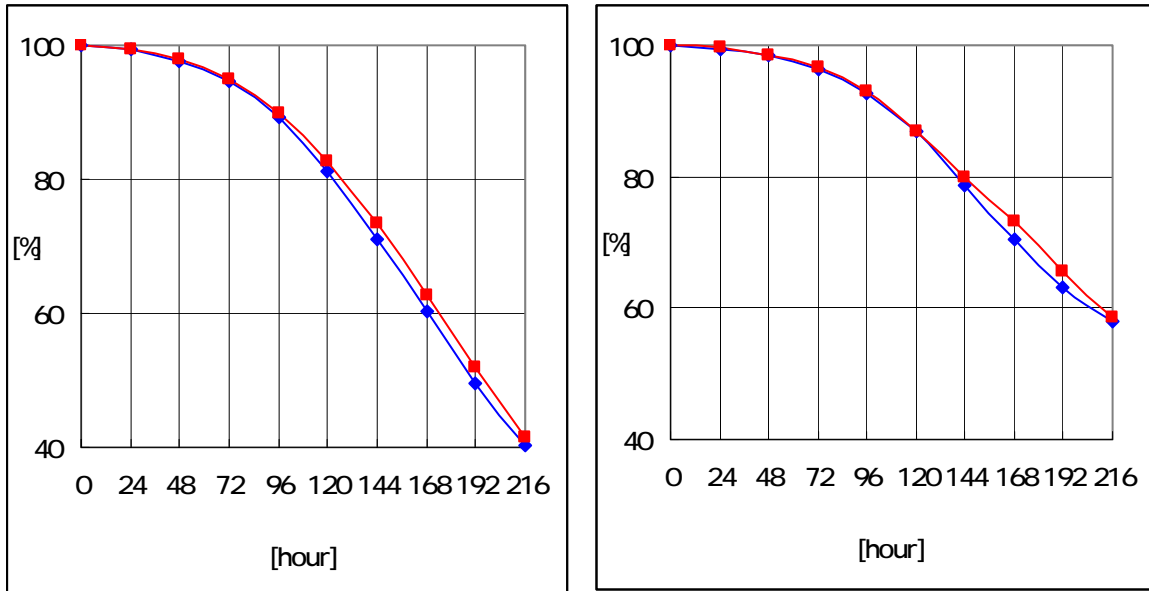


Fig.2 The comparison of the anomaly correlation (%) of 500hPa height forecasts in the Northern Hemisphere for August 2004 (left figure) and January 2005 (right figure) for each forecast hour. The red line means Test and the blue line indicates Cntl.

## A new thinning scheme based on one-hour time slots in 4D-Var for ATOVS assimilation

Hiromi Owada

Numerical Prediction Division, Japan Meteorological Agency

1-3-4 Otemachi, Chiyoda-ku, Tokyo 100-8122, JAPAN

email : howada@naps.kishou.go.jp

A thinning scheme based on one-hour time slots in the JMA operational global 4D-Var assimilation system was newly introduced into ATOVS radiance assimilation on 2 August 2005. Because the former thinning scheme suited for 3D-Var system was performed in the whole assimilation window of six hours, some overlapping data from multiple satellites were removed when their observation times differ by more than one hour. The new thinning scheme increases the number of ATOVS data used in the 4D-Var analysis by a factor of 1.5 in the polar regions. For AMSU-A from Aqua satellite whose orbit is mostly overlapped with NOAA-16, more data become to be used at low and mid-latitudes. To assess the impacts of the new scheme, one-month observation system experiments were performed for each of August 2004 and January 2005. The experiment for August 2004 demonstrated positive impacts on forecast skills as shown in Figure 1. In addition the quality of the typhoon track predictions was improved as in Figure 2. From the experiment for January 2005 impacts of the new scheme were globally neutral for the 500hPa geopotential height, but positive for the surface pressure (not shown).

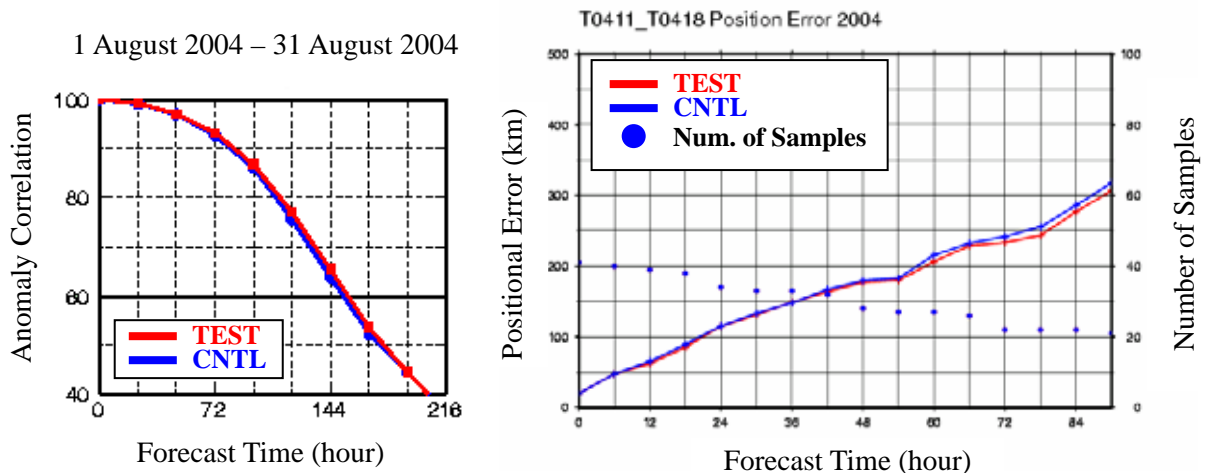


Figure 1 The global anomaly correlation for the 500hPa geopotential height verified against analysis. They are from 1st through 31st August 2004 for the new ATOVS thinning scheme (TEST) and the former scheme (CNTL).

Figure 2 Averaged typhoon track error in August 2004. Blue dots indicate the number of cases used in this statistics.



## Assimilation of space based GPS occultation data for JMA GSM

Eiji OZAWA<sup>(1)</sup>, Yoshiaki SATO<sup>(1)</sup>, Hideo TADA<sup>(2)</sup>, Yuichi AOYAMA<sup>(3)</sup>

(1) Numerical Prediction Division, Japan Meteorological Agency<sup>1</sup>

(2) Forecast Division, Japan Meteorological Agency

(3) National Institute of information and Communication Technology

### 1 Introduction

Methods to assimilate GPS occultation data are being developed at JMA. The GPS occultation data have high potential to improve initial field of the Global Spectral Model (GSM). GPS radio occultation data have various merits. For example, the sensors for GPS radio occultation are calibration free, data are globally distributed with very high-density in the vertical direction. Assimilation experiments with space based GPS data have been conducted for GSM of JMA using 3D-Var and 4D-Var systems.

### 2 Methods

CHAMP (Satellite Mini-satellite Payload) data sets are provided through the Internet by GFZ (GeoForschungsZentrum Potsdam). There are various methods for GPS data assimilation, such as assimilating excess phase, bending angle, refractivity, temperature and specific humidity. Among them, refractivity and bending angle assimilation are examined to determine which method is more beneficial. We conducted three experiments of “Cntl”(without GPS), “TEST1”(with refractivity), “TEST2”(with bending angles), then we compared the forecast scores and computational costs of these experiments using JMA 3D-Var system. The experiments using 4D-Var system were also conducted based on results of the assessment.

### 3 Results

The period of the 3D-Var assimilation experiments is July 2002, and those of the 4D-Var assimilation experiments are August 2004 and January 2005. Figures 1 show difference of RMS error of geo-potential height between TEST1 and CNTL. Figures 2 are same as figures 1 but compared with TEST2 and CNTL. These figures show little difference between TEST1 and TEST2, however bending angle assimilation has very high computational cost for our system. Taking into account this, the assimilation of refractivity is more effective for our system. As for refractivity assimilation using GSM 4D-Var system, forecast scores of geo-potential height and temperature from 850hPa to 300hPa are improved in winter season. In summer season however, the forecast scores both in the Southern Hemisphere and in the Tropics become worse. These results may suggest a need for adjusting the observation errors properly in the Tropics and

---

<sup>1</sup> Otemachi, Chiyoda-ku, Tokyo 100-8122, Japan  
E-mail: e-ozawa@naps.kishou.go.jp

other areas.

#### 4 Acknowledgements

To develop bending angle assimilation codes, we referred the codes provided by Zou et al.(1998) and Matsumura et al. (1999). The CHAMP data are provided by GFZ.(Wickert et al 2000a) We appreciate them.

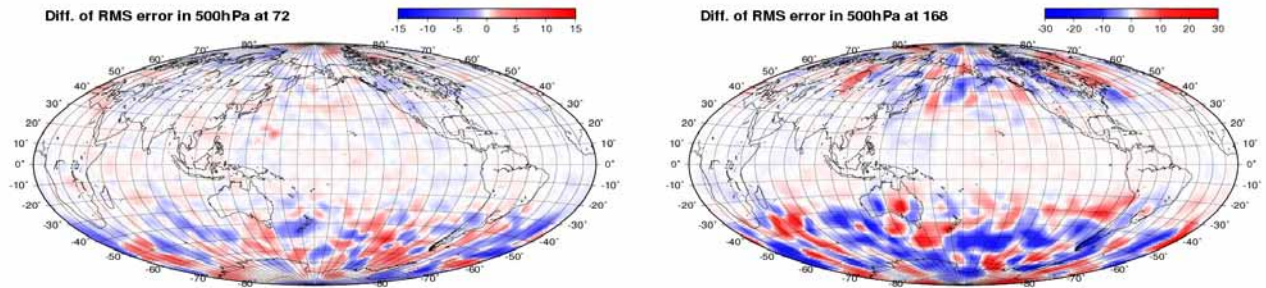


**Fig.1** Difference RMS error of geo-potential height in 500hPa between TEST1 and CNTL using GSM 3D-Var system. Left figure shows FT=72. Right Figure shows FT=168. Blue and red means improved and deteriorated area of RMS error respectively ( $RMS_{TEST1}-RMS_{CNTL}$ ).

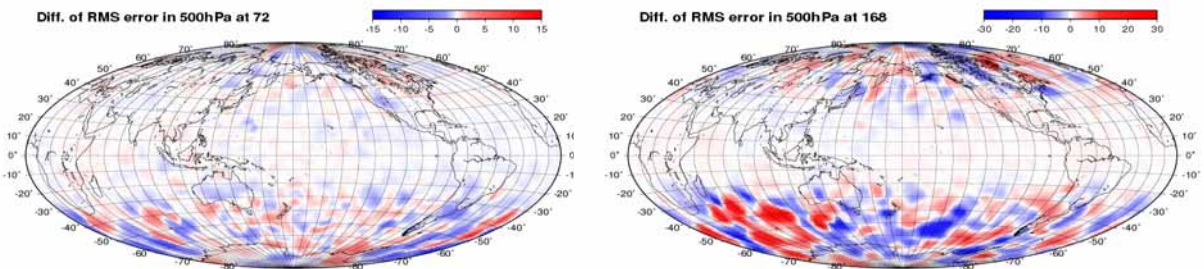


**Fig.2** Same as Fig.1, but for TEST2( $RMS_{TEST2}-RMS_{CNTL}$ ).

#### Reference

Matsumura T., Jhon C. Derber, James G. Yoe, Francois Vandenberghe, Xiaolei Zou(1999): The inclusion of GPS limb sounding data into NCEP's global data assimilation system, *NCEP office note*, **42**.

Wickert J. et al. (2000a), Atmosphere sounding by GPS radio occultation: First results from CHAMP, *Geophys. Res. Lett.*, **28**,3263-3266.

Zou, X., B. Wang, F. Vandenberghe, M.E.Gorbunov, Y.H.Kuo, S.Sokolovskiy, J.C.Chang and J.G.Sela (1998): Direct assimilation of GPS/MET refraction angle measurements Part : Variational assimilation using adjoint techniques. Submitted to *J.Geophys.Res.*.

## **Data assimilation scheme of satellite derived heating rates for soil state initialization in a regional atmospheric mesoscale model: methodology.**

Massimiliano Pasqui<sup>1\*</sup>, Robert L. Walko<sup>2</sup>, Stefano Migliorini<sup>3</sup>, Andrea Antonini<sup>1</sup>, Samantha Melani<sup>1</sup> and Gianni Messeri<sup>1</sup>

<sup>1</sup> *Institute of Biometeorology - National Research Council (IBIMET-CNR), Florence, Italy*

<sup>2</sup> *Department of Civil and Environmental Engineering, Duke University, Durham, North Carolina, USA*

<sup>3</sup> *Data Assimilation Research Centre, Department of Meteorology, University of Reading, Reading, UK*

*\*Corresponding Autho: m.pasqui@ibimet.cnr.it*

An alternative satellite data assimilation method has been developed, for the Regional Atmospheric Modelling System (RAMS), which incorporates satellite – observed heating rates in order to retrieve soil moisture. It is based on the new generation of geostationary Meteosat Second Generation data, taking advantage of their enhanced spatial and temporal resolution.

The method acts on the soil moisture in RAMS ground levels adjusting it, upward and downward, until the RAMS simulated surface heating rate is in close agreement with the satellite – observed one in each grid cell. The method simply carries out a forward integration of the Soil – Vegetation – Atmospheric RAMS component (the Land Ecosystem Atmosphere Feedback version 2 model, LEAF2) for a special assimilation period in order to adjust the model soil moisture according with the observed data. Iterations needed add just a small amount of time to be computed to the total simulation time.

Surface soil water content can be measured using remote sensing instruments operating at low microwave frequencies (typically less than 10 GHz). Forthcoming satellite-borne instruments – such as the Advanced Microwave Scanning Radiometer (AMSR-E) and the Soil Moisture and Ocean Salinity Sensor (SMOS) - are about to provide surface soil moisture measurements at global scale. However, the low-frequency spectral band of the sensors and the polar-orbiting configuration of the satellites will not give rise to neither spatial nor temporal high-resolution measurements.

A possible alternative that complements a direct measurement of soil moisture is the assimilation of heating rates from a geostationary satellite in a land surface model. Satellite data can be used to infer the partitioning between latent and sensible heat fluxes, taking into account the influence of vegetation on the surface energy budget (McNider et al.1994).

Heating rates are derived from the Meteosat 8 SEVIRI thermal infrared channels (10.8 and 12 micron), which provide an estimate of the surface skin temperature at 3 km (at Nadir) spatial and 15 min. temporal resolution. Raw data over land are resampled at the model resolution and the satellite heating rate estimate for each model grid-box is calculated by estimating the satellite-derived surface temperature temporal gradient over three consecutive SEVIRI acquisitions.

Assimilation is performed during the mid-morning, period in which change in surface temperature is more sensitive to soil moisture than to other components in the surface energy budget.

It is important to note that such technique is especially suited for geostationary satellite acquisitions, since morning periods of maximum solar heating rate are not well covered by polar satellites passages. Furthermore, heating rates derived from different radiometers would suffer from inter-calibration discrepancies, which can be non-negligible in this kind of application and spoil the benefits of assimilation. Finally, the SEVIRI high measurement repetition rate and spatial resolution helps us minimize the number of pixels affected by clouds.

The assimilation approach presently implemented, described in the following paragraph, has the advantage of being conceptually very simple and constitutes a first step for assessing the potential benefits of assimilation of soil moisture for improving medium-range NWP forecasts. Future work will involve the development of a more sophisticated assimilation scheme with a proper treatment of observation and forecast errors. A possible candidate is the Ensemble Kalman Filter methodology, which does not require coding the adjoint of the model: the moderate number of variables in a land surface model makes the technique feasible despite its high computational cost (Crow and Wood, 2003).

The method is in principle the same as the method implemented by Jones et al. 1998a and Jones et al. 1998b in which soil moisture in RAMS is adjusted upward or downward until the RAMS-simulated surface heating rate is in close agreement with the satellite-observed surface heating rate in each grid cell. However, there are many differences in how the scheme is implemented. Jones et al. 1998a, inverted many of the prognostic equations in the RAMS land surface model in order to derive a direct expression for the change of soil moisture that would lead to the desired change in modelled surface heating rate (to match observed values). A complete nonlinear analytic inversion was not possible, so a few iterations (usually 3 to 5) were required to achieve convergence.

The present method is much simpler to implement because it requires no inversion of the model equations. It simply carries out a forward integration of all or part of the model for a special assimilation period, usually about 1 hour, compares the model and observed surface heating rates, adjusts soil moisture upward or downward based on this

comparison, and repeats the process. Each successive iteration, the moisture adjustment is smaller, and if 7 iterations are carried out, soil moisture will always be adjusted to within 1% of the "correct" assimilation value. This approach is very flexible and has many advantages over the approach taken by Jones et al. For one thing, one can very easily vary which processes are active or inactive in the model during the assimilation cycle. For example, one can include full atmospheric processes in the cycle, including precipitation, or one can hold atmospheric variables constant and only predict land surface and soil properties. Also, one can vary the relative adjustment of soil moisture as a function of depth in the soil, for example in case one wants only to modify shallow but not deep moisture in the assimilation process. A new derivation would be required of the equation set for each of these modifications if the inverted equations were to be used. Moreover, if the complete atmospheric model is included in the assimilation cycle, inversion of all equations is very complicated (this constitutes a full adjoint of the model, which is under development in other work). Probably the only disadvantage of the present method is the requirement of more iterations to achieve convergence, but even with twice as many iterations required, the entire assimilation process with only the land surface model active (as done in Jones et al.) adds less than 10% to the total computation time of most forecasts, and less than 5% in many cases.

A more important reason for using the present method is that the present land surface model in RAMS, which is called LEAF2, is very different from the earlier version used in the study of Jones 1998a.

One of its special features is representation of multiple landuse types in a single surface grid cell by dividing the cell into subgrid patches. Energy and water of soil, vegetation, temporary surface water, and canopy air are prognosed separately in each patch, and surface fluxes are evaluated between each patch and the overlying atmospheric column.

The present soil moisture adjustment process is carried out in the following way: the RAMS simulation is begun in a normal way, beginning from initial conditions and integrating forward in time for a few hours. At a specified time in the simulation which we denote here as TA1, usually chosen to be approximately 9 or 10 A.M. local time when surface warming from solar radiation is rapid, the model forward integration is temporarily halted and the assimilation process is carried out. The assimilation process involves a series of forward integrations of the surface model (LEAF2 only, with atmospheric conditions held constant in time) for a period of 1 hour, from TA1 to TA2. In the first iteration of the assimilation cycle, the forward integration of the surface model is initialized using current soil moisture values, WGP from the RAMS forecast. Then, for each grid cell, the average modelled surface heating rate over the period from TA1 to TA2 is compared against the observed value. Next, LEAF2 is reinitialized at TA1 for the second iteration. If on the previous iteration the model heated up more quickly than observation, soil moisture at TA1 is set to a value half way between WGP and WMAX, where WMAX is the maximum possible soil moisture content. If the model heated up more slowly than observation, soil moisture at TA1 is set to a value half way between WGP and WMIN, where WMIN is the minimum possible soil moisture content. The second forward integration to TA2 is carried out with LEAF2, and model heating rates are again compared with observation. To begin the third forward integration of LEAF2 from TA1 to TA2, soil moisture is adjusted upward or downward from the initial value on the previous iteration by 25% of the range (WMAX - WGP) or of the range (WGP - WMIN) based on this comparison. For the fourth iteration, the moisture adjustment is an increase or decrease of 12.5%, continuing with half the adjustment magnitude each iteration. Following the eighth iteration, the final moisture adjustment is about 0.4%, and the LEAF2 soil moisture values, WGP, are set to the assimilated values. Then, the model simulation proceeds forward from TA1 using the adjusted soil moisture.

In the assimilation code a weighting factor (WF), with values ranging from 0 to 1, is defined as a function of depth in the soil and is used to control the relative amount of soil moisture adjustment performed at each level in the soil, in case it is desired to not adjust uniformly at all levels. The soil moisture adjustment process is carried out as described above for any soil level  $k$  that has the  $WF = 1$ , and no adjustment is done for levels where  $WF = 0$ . Because shallow moisture in the soil usually impacts surface fluxes more than does deeper moisture, and because it may be desirable to minimize the total impact of the soil moisture adjustment process on the total water content of the soil, it has been defined a WF profile that is 1 at the surface, decreases linearly to 0 at a depth of 2/3 meter, and remains at 0 below that. It would be worthwhile to experiment with this weight profile in an operational setting.

Besides being very simple to implement, this method also allows considerable flexibility. For example, it is possible to modify soil moisture at all levels, or instead limit the adjustment to the shallower layers, knowing that the latter are the most influential in determining surface heating rate. It is possible to hold the atmospheric conditions constant and only integrate the soil model during the assimilation cycle, or let the atmosphere respond to the changed soil moisture and feed back to the surface temperature during the assimilation cycle. Each of these choices can be implemented with a few IF statements in the code without any need for re-inverting the equation set each time and is thus a very attractive approach. Furthermore the method can be expanded to many other aspects of initialization of critical initial fields such as atmospheric liquid and ice content.

This strategy is under a deep testing phase, preliminary results seem promising thus encouraging not only an operational usage, but also for seasonal studies.

## A SOIL MOISTURE INITIALIZATION METHOD, BASED ON ANTECEDENT PRECIPITATION APPROACH, FOR REGIONAL ATMOSPHERIC MODELING SYSTEM: A SENSITIVITY STUDY ON PRECIPITATION AND TEMPERATURE.

Massimiliano Pasqui<sup>1\*</sup>, Craig J. Tremback<sup>2</sup>, Francesco Meneguzzo<sup>1</sup>, Graziano Giuliani<sup>1</sup> and Bernardo Gozzini<sup>1</sup>

<sup>1</sup> Institute of Biometeorology - National Research Council (IBIMET-CNR), Florence, Italy

<sup>2</sup> Atmet, LLC, Boulder, Colorado

\*Corresponding Author: m.pasqui@ibimet.cnr.it

The soil initialization state is very important on a wide range of behavior in weather forecast but availability of such information as first guess field is difficult. The new version of RAMS provides a method to produce initial soil state computed from simulated atmospheric and observed precipitation fields. In other words it is possible to run the LEAF model prescribing both the atmosphere state and rainfall, which, for example, could be the observed one. The atmosphere state is provided by a previous atmospheric RAMS simulation. It is clear that if an observed rainfall is used to force the water budget, the atmospheric forcing is not identical to the real one that produces the observed rainfall ingested. Differences in water exchange between soil – vegetation – air between the real one and the simulated could be important. But such soil first guess field possesses some benefit like, a better realism on the evaluated water amount respect to what is just forecasted, better description of heterogeneity due to the acting hydrology model within LEAF, longer description of water cycle forcing respect to a simple initial estimation of soil state retrieved, for example, by a satellite. The soil initialization scheme is based on a special version RAMS called RAPI (RAMS Antecedent Precipitation Index). The RAPI model needs two different types of input:

1. *Precipitation Fields*: a distributed map of rainfall over the interest area and the selected time period (satellite estimates);
2. *RAMS Atmospheric Fields*, computed in a separate RAMS run on the same time period.

Using such information RAPI model computes energy balance, as the RAMS actually does, between atmosphere, prescribed from a previous RAMS run, and the provided rainfall fields. A complete strategy scheme is presented in fig 1. Using the observed rainfall has the advantage of computing a better and realistic water budget, at soil level, both for heterogeneity and reliability. Several benefits of using RAPI, both from a physical and an operational point of view, should be highlighted:

- The provided information on observed precipitation, using a simple preprocessing tool, is projected on a regular RAMS grid thus at the same resolution of the simulation. The observed precipitation should be provided on a regular Lat/Long area covering the interest area. The RAMS standard method for ingesting geographical information such as Sea Surface Temperature or Soil/Vegetation Dataset, is used providing a simple way for data input.
- The observed precipitation, once projected on the interest area, possesses the same topography as model grids, so a basin budget could be more reasonable than soil moisture or temperature interpolation coming from a coarser grid simulation (e.g. a GCM field).
- This method could be simply nested, in time, in order to build up budget over long period. Subsequent simulation could be “*appended*” in the operational production cycle providing the continuity of the soil state information flow, describing in a proper way the long term behavior of soil.
- Due to the reduced number of equations solved in the model system, the RAPI run is computationally efficient.
- The method does not need only “*full real-time*” observed precipitation, because RAPI could be run, for example, at the end of a day in order to provide initial soil state for the following day simulation. So a simple RAPI use in an operational chain is possible.

The RAMS simulation has performed on a 2002 summer period in order to stress the soil influence on low level atmospheric behavior and, in order to explain how the RAPI model works, a brief step by step description is presented here.

The RAMS simulation was performed using a 3 nested grids configuration at 32 – 8 – 2 km of horizontal resolution and 36 vertical levels with a resolution ranging from 50 m to 1100 m and 11 ground level down to -1.5 m with a stretched resolution. Initial and boundary conditions, every 6 hours, were from NCEP/NCAR reanalysis fields, Kalnay et al. (1996), while sea surface temperature, at 1° of resolution, were the weekly mean Reynolds reconstructed SST from NOAA. Initial soil condition was set as a standard operational run as follows:

- *Initial Soil Temperature:* it is set with an initial offset of the lower level atmospheric temperature, ranging between 1 and -1 °C (from top to bottom level) homogeneously distributed over the whole area. This is the standard soil RAMS initialization.
- *Initial Soil Moisture:* it is set to a typical medium - dry soil prescribed value, equal to 0.04. This is the fraction of total soil volume that is not occupied by solid soil particles (i.e., it is the fraction of total soil volume that is occupied by air plus water). Such value is the initial prognostic soil moisture, which is in units of cubic meters of water per cubic meter of total volume, where that total volume is comprised of water plus air plus solid soil particles. Therefore such value is soil type dependent.

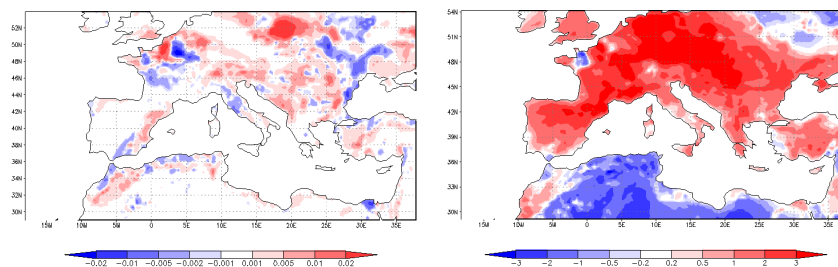


Fig 1 Initial soil moisture and temperature difference, expressed cubic meters of water per cubic meter of total volume, where that total volume is comprised of water plus air plus solid soil particles, on the coarser grid at 3<sup>rd</sup> Aug 2002, 00 UTC.

In this work a new possible application of RAMS model is presented and explained using a summer 2002 case study. Only qualitative evidence of possible impacts are shown while, for quantitative estimates of benefits further study should be done. The simple usage of the RAPI model to build up reasonable the soil state as first guess field, encouraging a large range of application, from now-casting to regional climatic purposes. The RAPI model could be an important tool in order to estimate the soil wetness thresholds for hydrological application, especially for supporting the river basins monitoring systems.

# Data Assimilation Experiments of Vertical Gradient of Refractivity Observed by Wind Profiler Network

Hiromu SEKO<sup>\*1</sup>, Jun-ichi FURUMOTO<sup>2</sup>, Masahiro SASAOKA<sup>1</sup>, Kazuo SAITO<sup>1</sup>, Tadashi TSUYUKI<sup>3</sup>

<sup>1</sup> Meteorological Research Institute, Japan Meteorological Agency, Tsukuba, Japan

<sup>2</sup> Research Institute for Sustainable Humanosphere, Kyoto University, Kyoto, Japan

<sup>3</sup> Numerical Prediction Division, Japan Meteorological Agency, Tokyo, Japan

## 1. Introduction

The Japan Meteorological Agency (JMA) deployed the nation wide network of wind profiles (WINDAS) to observe the mesoscale airflow distribution. Because the horizontal wind observed by the WINDAS helps to specify the position of the low-level convergence, the accuracy of the rainfall forecast was improved when these data were used as assimilation data. Besides the convergence of the airflow, water vapor plays important roles on the generation or development of heavy rainfalls, i.e., the abundant supply of low-level humid air causes heavy rainfalls and the middle-level dry air affects the development of the convection. The vertical profiles of water vapor are conventionally observed by the rawinsonde. However the time interval of the rawinsonde observation was as long as 12 hour, and then rawinsonde data does not necessarily catch the mesoscale severe phenomena whose time scale is generally less than 12 hours.

Recently, the estimation method of the vertical gradient of refractivity from the wind spectrum and signal-to-noise ratio observed by wind profiler was developed through the feature of the turbulence echo that depends on the vertical gradient of refractivity (e.g. Tsuda et al., 2001). When these data observed by WINDAS are used as assimilation data, the accuracy of the rainfall forecast is expected to be improved.

In this study, the vertical refractivity profiles were estimated from the WINDAS data and the impact of these data was investigated by using the Meso-4DVar Data assimilation system of JMA (Koizumi et al., 2005).

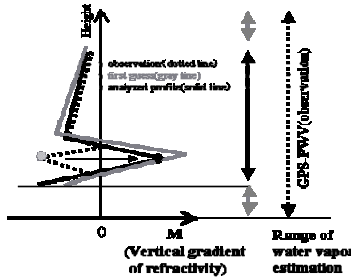


Fig. 1 Schematic illustration how to determine the sign of vertical gradient of refractivity

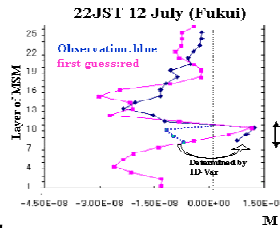


Fig. 2 vertical profile of gradient of refractivity at 22JST 12 July at Fukui

## . Vertical profile of the water vapor

In the estimation of vertical gradient of refractivity, we followed the method of Sasaoka (2003). Namely, the vertical gradient of refractivity was estimated using next relations;

$$|M| = \alpha |\varepsilon|^{-1/3} |N| \eta_{turb}^{1/2}$$

$$\varepsilon = 0.5N(\sigma_{turb}/2)^2$$

$$\eta_{turb} = 10^{0.1SNR}$$

where  $M$  is the vertical gradient of

refractivity,  $SNR$  the signal-to-noise-ratio,  $\sigma_{turb}$  the width of the spectrum and  $N$  the Brunt-Visala frequency.

Firstly, the profile of  $M$  was calculated with the vertical resolution of MSM (JMA operational hydrostatic Mesoscale model).  $\alpha$  was determined so that the sum of the absolute value of  $M$  was equal to one calculated from the first guess, which was the outputs of MSM. The sign of the vertical gradient was not determined by the observation. Thus, one-dimensional variational analysis (1DVar) was performed to determine the signs of  $M$ . When the number of layers where  $M$  is positive was investigated using the rawinsonde data at Wajima during July 2004, a few layers are positive at the maximum. So, the combination of the signs that minimizes the following cost function was found by changing the sign of  $M$ .

$$J = \frac{1}{2} \sum (M - M_g)^2 + \frac{1}{2} \sum_{inside\ of\ obs.\ range} (M - M_{obs})^2 + \frac{1}{2} \left( \sum_{inside\ of\ obs.\ range} \rho_g q_g \Delta z + \sum_{outside\ of\ obs.\ range} \rho_g q_{vg} \Delta z - PWV \right)^2$$

where  $\rho$  and  $q_v$  is the density and mixing ratio of water vapor, respectively.  $PWV$  is GPS-derived precipitable water vapor, which was obtained by interpolation of  $PWV$  data of GEONET. The suffix  $g$  indicates first guess

\* hseko@mri-jma.go.jp, phone +81-29-853-8640; fax +81-29-853-8649

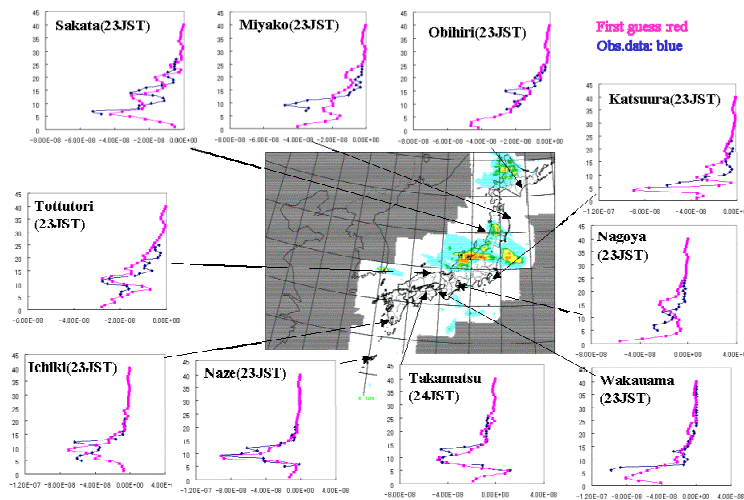


Fig. 3 Precipitation and vertical profiles of vertical gradient of refractivity at 23JST 17 July 2004.

which is the stationary front extending from China to Japan in early summer, crossed the central Japan. Figure 3 shows precipitation distribution and the vertical gradient profiles of the refractivity observed by WINDAS. At 23JST, the well-developed line-shaped convective band crossed the central part of Japan and wide weak precipitation region existed on the northern side of the band. This convective band was developed by the low-level southwesterly flow over the Sea of Japan (not shown). On the southern side to the convective band (e.g., Ichiki, Naze and Takamatsu), the profiles of vertical gradient were similar to those of first guess. There was a layer with the minimum vertical gradient at the height of  $k=10$ . This minimum layer indicates the top of the boundary layer where the water vapor changed drastically.

These gradient data were assimilated into MSM. The grid interval of 10 km was adopted to resolve the mesoscale convective systems that caused the heavy rainfall. When the vertical gradient was assimilated, the precipitation region extended westward. However, this distribution was different from the observed one.

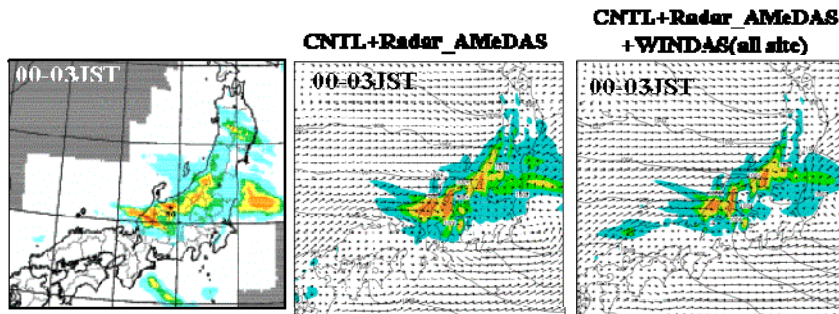


Fig.4 Observed precipitation during 00-03JST 17 July 2004 and the precipitation predicted from the assimilated fields of (left) conventional data and radar AMeDAS precipitation, and (right) convective data and all wind profiler data.

The accuracy of the observed vertical gradients of refractivity should be investigated and further data assimilation experiments should be conducted to reduce the observation error.

### References

Koizumi, K., Y., Ishikawa and T. Tsuyuki; Assimilation of Precipitation Data to the JMA Mesoscale Model with a Four-dimensional Variational Method and its Impact on Precipitation Forecasts, 2005; *Sola*, 1, 45-48.  
 Sasaoka, M., Estimation of water vapor profile in the convective boundary layer, 2003; *Proc. of the Autumn Conference of J. Meteor. Soc.*, **84**, 310, (in Japanese).  
 Tsuda, T., M. Miyamoto and J. Furumoto (2001): Estimation of a humidity profile using turbulence echo characteristics. *J. Atmos. Oceanic Technol.* **18**. 1214-1222.

value.

One example of the results of the 1DVar analysis is shown in fig. 2. The vertical profile of  $M$  whose sign was determined by 1DVar became close to that of the first guess. This profile indicates that the 1DVar analysis determined the signs of observed  $M$  correctly. The temperature and mixing ratio of water vapor can be estimated by the 1DVar analysis. However, the observed  $M$  whose sign was changed by the 1DVar was used as assimilation data.

### 3. Impacts of the vertical gradient of refractivity profiles observed by WINDAS

On 17-18 July 2004, the Baiu front,

### 5. Summary

The vertical gradient of the refractivity was estimated from WINDAS data. When the observed gradient was compared with the first guess, the feature of the boundary layer was similar to the observed ones in the upstream side of the low-level inflow. However, when this data were assimilated into MSM, the precipitation regions extended westward and the predicted precipitation distribution was different from the observed one.

# Data Assimilation Experiments using CHAMP Refractivity Data

Hiromu SEKO<sup>\*1</sup>, Yoshinori SHOJI<sup>1</sup>, Masaru KUNII<sup>1</sup>, Kazuo SAITO<sup>1</sup>, Yuichi AOYAMA<sup>2</sup>

<sup>1</sup> Meteorological Research Institute, Japan Meteorological Agency, Tsukuba, Japan

<sup>2</sup> National Institute of Information and Communications Technology, Koganei, Japan

## 1. Introduction

It is well known that the abundant supply of low-level water vapor causes the heavy rainfalls and the middle-level water vapor also affects the development of the convection. Therefore the prediction of heavy rainfall events is expected to be improved when the vertical profile of water vapor is the assimilation data. The vertical profiles of water vapor can be obtained by rawinsonde. However, the position of rawinsonde data existed only on land except for the several points in oceans observed by meteorological vessels. Because Japan was surrounded by oceans, the humid airflow from the ocean often caused the heavy rainfalls. So, the observation of the vertical profile over the sea is desired. Recently, the refractivity profile estimated from the occultation data of a low earth orbit (LEO) satellite CHAMP launched by GeoForschungs Zentrum Potsdam (GFZ) ) became available. In this study, the impact of the refractivity data on the prediction of the heavy rainfall is examined.

## 2. Numerical model and refractivity data observed by CHAMP

CHAMP receives the signal transmitted from the Global Positioning System (GPS) satellites which are rising from or sinking to the earth. Thus, the occultation data have the information along the path of the signal that slices the atmosphere. The general estimation procedures of occultation data are as follows; (1) the angle bended by the atmosphere is estimated from the temporal variation of the signal delay which was caused by the atmosphere, and then (2) the profiles of refractivity are estimated from the bending angles. So far, it was shown that the forecast was improved when the bending angle data was assimilated into the Global Spectrum Model of JMA (Ozawa et al. 2005). In this study, the refractivity profile of the data was assimilated into the Meso-scale Spectrum Model (MSM) of JMA by using the Meso-4DVar Data Assimilation System (Koizumi et al., 2005). MSM is the operational hydrostatic model to perform the short-range forecast of the severe weather. A grid interval of 10 km was adopted to resolve the mesoscale convective systems that caused the heavy rainfall.

We used the refractivity profile data estimated by GFZ. Firstly, the D-value, which is the difference of the observation and first guess value, was investigated. The field predicted by MSM was used as the first guess value. Figure 1 shows the position of CHAMP data in July 2004. The area indicated by blue rectangle is the domain of MSM. The average and RMS profiles are shown in fig. 2. The number of data was decreased at the lower layer and the bias and RMS are large below the height of 2km. Therefore, the data above the height of 2km were used as the assimilation data.

## 3. Impacts of RW and GPS-derived PWV

On 16 July 2004, Baiu front, which is the stationary front extending from China to Japan in the early summer, crossed the northern Japan. At about 12JST (Japan Standard time, 9JST corresponds to 0UTC), the observation point, which was the nearest point to the earth on the path, passed through the Baiu front. The profiles of the refractivity are shown in fig. 3. The refractivity below the height of 4 km was larger than that of the first guess value. When these data were used, the water vapor below the height 2 km is expected to be increased.

Left panels of fig. 4 show the precipitation region observed by the convective radars. Besides the precipitation along the western coast lines, the intense convective band associated with the Baiu front crossed the northern Japan. This convective

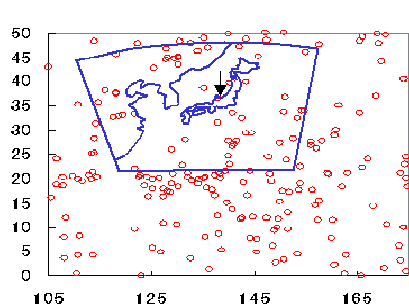


Fig.1 Distribution of CHAMP data in July 2004. Black arrow indicates the position of data that was assimilated into MSM

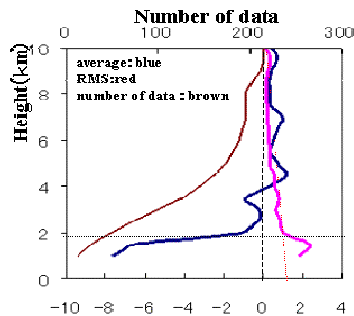


Fig.2 Vertical profile of average, RMS and data number of CHAMP data

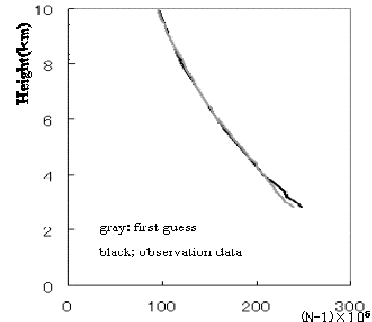


Fig.3 Vertical profile of CHAMP data and first guess data on 16 July 2004

\* hseko@mri-jma.go.jp, phone +81-29-853-8640; fax +81-29-853-8649

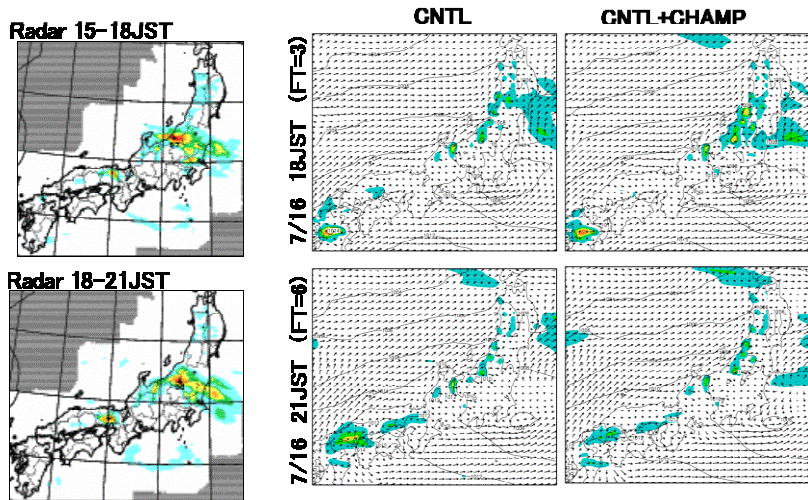


Fig.4 (Right) Observed precipitation and (center and right) precipitation predicted from the initial fields, into which (center) convective data and (right) conventional data and CHAMP data were assimilated

data and convective data were used, the precipitation region was more similar to the observed one and precipitation became more intense, although the precipitation was not maintained until FT=6hour in the both cases.

One of the merits of occultation data is the high vertical resolution. Additional experiments were performed by changing the vertical resolution of data and eliminating the lowest data. When the vertical resolution of the refractivity data was set to be 600 m that is three times of the aforementioned ones, the precipitation region became smaller. When the lowest data of the observed refractivity profile were further removed from the assimilation data, the precipitation region was more close to the only-conventional-data-assimilated case. This result indicates that (1) the optimal vertical resolution should be considered in the assimilation and (2) the lowest data are important for the prediction of the heavy rainfall because the data in low-layer have information of the low-level humid air supply.

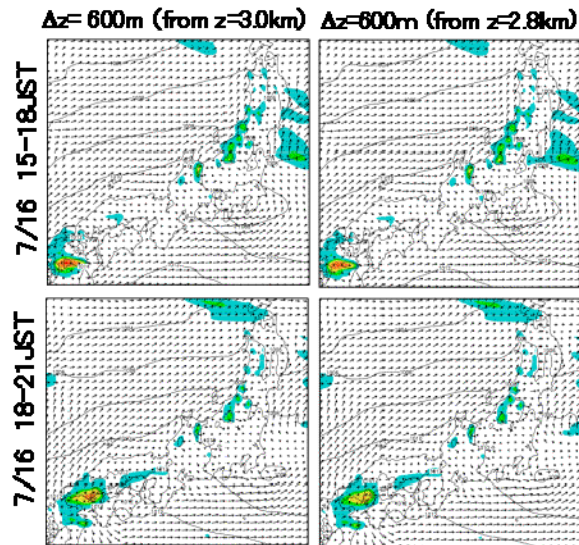


Fig.5 Same as fig. 4 except the vertical data resolution.

band maintained without decaying until 21JST. Right panels are precipitation regions simulated by MSM. The initial condition of MSM was produced by the assimilation of the convective data and the CHAMP-derived refractivity data. In this case, two assimilation windows from 9HST to 12JST and 12JST to 15JST were used. The analyzed fields of 15JST were used as the initial data. The observation error of the CHAMP-refractivity data was proportional to the RMS profile of the d-value. Its absolute value was determined by trial and error.

When the convective data were assimilated, the position of precipitation region was shifted northward and precipitation intensity was weaker than the observed one. When the CHAMP

#### 4. Summary

When the CHAMP-derived refractivity data was assimilated, the precipitation regions became similar to the observed ones and the precipitation intensity also became more intense. Thus, the CHAMP-derived data have potential to improve the rainfall forecast. To reduce the observation error, the number of data should be increased. The vertical correlation of observation error should be also investigated to make the best use of the vertical high-resolution data.

#### Acknowledgments

CHAMP data were provided from GFZ. The initial and boundary conditions of MSM were provided from the Numerical Prediction Division (NPD) of JMA. We also used MSM and Meso-4DVar system developed by NPD/JMA. We would like to thank Dr. Wickert of GFZ and members of NPD/JMA.

#### References

- Koizumi, K., Y., Ishikawa and T. Tsuyuki; Assimilation of Precipitation Data to the JMA Mesoscale Model with a Four-dimensional Variational Method and its Impact on Precipitation Forecasts, 2005; *Sola*, **1**, 45-48.
- Ozawa, E, Y. Sato, H., Tada and Y., Aoyama, Assimilation of space based GPS occultation data for JMA GSM, 2005, *CAS/JSC WGNE Research Activities in Atmospheric and Oceanic Models*, **36**, (in this volume)

# Assimilation of GPS Radio Occultation Observations

Hui Shao<sup>1</sup> and Xiaolei Zou<sup>2</sup>

<sup>1</sup>Center for Ocean-Atmosphere Prediction Studies, Florida State University, Tallahassee, FL, USA

<sup>2</sup>Department of Meteorology, Florida State University, Tallahassee, FL, USA

(shao@coaps.fsu.edu, zou@met.fsu.edu)

In a local refractivity assimilation (Kursinski et al 2000, Poli et al 2002), a simulated refractivity profile is interpreted as a vertical profile at the averaged position of all tangent points of a radio occultation (RO). In the bending angle assimilation, the along-track refractivity and its gradient determines the bending of each individual ray-path through the integration of the ray-trajectory equation (Zou, 1999). The bending angle calculated from such an operator is physically consistent to the way the Global Positioning System (GPS) RO observations are obtained and processed. Such a consistency renders the bending angle assimilation more desirable when accuracy is a priority. However, the integration of the ray-trajectory equation is expensive, especially for its applications in operational weather forecasts. Aiming at achieving both accuracy and computational efficiency, a new observation operator that simulates the GPS excess phase delay was proposed and tested for GPS RO data assimilation. The GPS excess phase delay is approximated in the assimilation forward operator as a integration of the local refractivity along the tangent link of a ray-path of the radio signal transmitted from a GPS satellite to a low Earth Orbit (LEO) satellite, occulted by the Earth (Figure 1).

The National Centers for Environmental prediction (NCEP) spectral statistical interpolation (SSI) system at a resolution of T170L42 was used. The forward operator and its adjoint model for the assimilation of the excess phase delay were developed and incorporated. The forward simulation and assimilation experiments using the system were conducted (PHA) for the time period from May 20 to 31, 2002. A total of 1158 the German CHALLENGING Minisatellite Payload (CHAMP) RO sounding observed in the time window during the period were used. Two more experiments, local refractivity simulations and assimilations (REF) and a control run without the assimilation of GPS data (NOGPS) were also carried out. The results from PHA, REF and NOGPS were compared. Based on the same background of refractivity, the excess phase delay simulated by PHA has less bias from its observation value than the local refractivity simulated by REF from its observation (Figure 2). After assimilations of GPS data, PHA results in a smallest bias of the GPS refractivity than REF and NOGPS, indicating that the analysis from PHA is more accurate than those from the other two experiments. The impacts of the assimilation of the excess phase delay observations were studied in terms of both the general statistical mean and STD and case studies. We found that PHA tends to produce a warmer and moister atmosphere than REF. It also introduces a finer structure with a larger radius of influence to the temperature and specific humidity analysis fields (Figure 3 and 4).

Under the assumption of the spherical symmetry of the local refractivity, an alternative form of the excess phase delay, symmetric excess phase delay, and its observation operator were derived. Simulation and assimilation experiments using the forward operator were carried out (PHA-sym). It shows that PHA-sym produces intermediate results between PHA and REF. Since it is simpler than PHA, and meanwhile keeps most information for the alongtrack refractivity gradients, it may be more desirable in a operational numerical model implemented via a localized parallel algorithm without any changes of the model structure. However, when and where this symmetric excess phase delay can substitute the excess phase delay are yet to be studies further.

-----  
Computations were performed on the IBM SP4 at the FSU. GPS radio occultation data were provided by COSMIC at UCAR. This research was supported by NSF project: ATM-0101036.

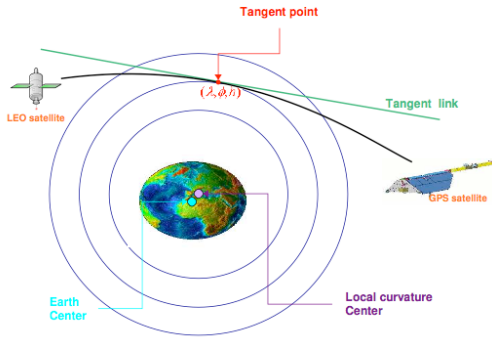


Figure 1: Schematic illustration of the definition of a tangent link. Assume the earth is an ellipsoid. Given a GPS measurement at a tangent point  $(\lambda, \phi, h)$ , a tangent line (referred to as the tangent link) is constructed so that it goes through the point  $(\lambda, \phi, h)$ , tangent to the local curvature and coplanar to the plane containing the GPS and LEO satellites (occultation plane).

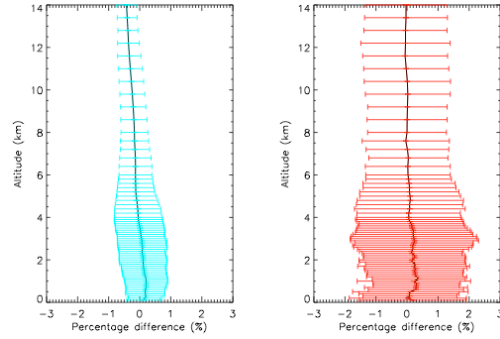


Figure 2: Vertical profiles of the mean and standard deviation (error bars) of fractional difference between the simulation and the observed values of GPS excess phase delay (left panel) and local refractivity (right panel). The quantities are calculated from 1158 simulated soundings during May 24-31 2002.

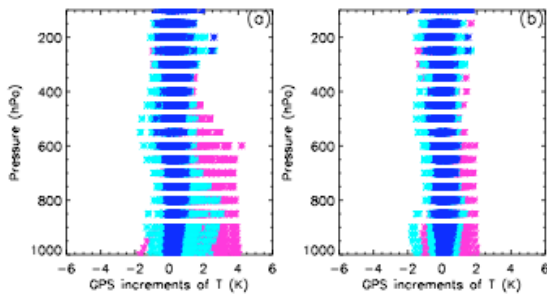


Figure 3: Spaghetti plots of the GPS increments of T for (a) PHA and (b) REF. The profiles have been color-coded according to their corresponding occultation latitudes: blue represents soundings in the tropics ( $30^{\circ}\text{S} - 30^{\circ}\text{N}$ ), cyan represents soundings in mid-latitudes ( $30^{\circ}\text{S} - 60^{\circ}\text{S}$  and  $30^{\circ}\text{N} - 60^{\circ}\text{N}$ ) and magenta represents soundings in high-latitudes ( $60^{\circ}\text{S} - 90^{\circ}\text{S}$  and  $60^{\circ}\text{N} - 90^{\circ}\text{N}$ ).

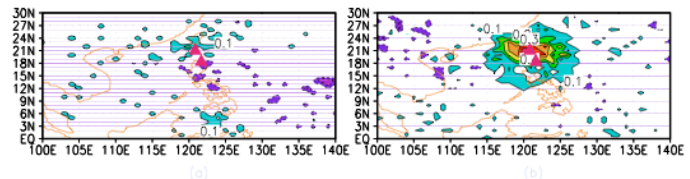


Figure 4: Distribution of the GPS increments of the 850hPa specific humidity in the subdomain ( $10^{\circ} - 140^{\circ}\text{E}$ ,  $90^{\circ} - 10^{\circ}\text{S}$ ) at 06UTC May 30, 2002 for REF (left panel) and PHA (right panel). The triangles indicate the GPS occultation points.

## References

- Kursinski E. R., S. B. Healy, and L. R. Romans. Initial results of combining GPS occultations with ECMWF global analyses within a 1dvar framework. *Earth Planets Space*, 52:885–892, 2000.
- Poli P., J. Joanna, and E. R. Kursinski, 1DVAR analysis of temperature and humidity using GPS radio occultation refractivity data. *J. Geoph. Res.*, 107(D20), 4448, doi: 10.1029/2001JD00935, 2002.
- Zou X., F. Vandenberghe, B. Wang, M. E. Gorbunov, Y.-H. Kuo, S. Sokolovskiy, J. C. Chang, J. G. Sela, and R. A. Anthes. A raytracing operator and its adjoint for the use of GPS/MET refraction angle measurements. *J. Geophys. Res.*, 104:22,301–22,318, 1999.

# Development of a 3-D spatial ARMA-filters based analysis scheme

M.Tsyarulnikov<sup>1</sup>, P.Svirenko, R.Zaripov

*Russian Hydrometeorological Center*

## 1 Introduction and general design

A new 3-D meteorological data assimilation scheme is being developed in the RHMC. The principal features required of the scheme are:

(1) The scheme is intended to be as universal as possible. First, it should be applicable for data assimilation on all spatial scales (global, regional, and meso-scale). Second, the core of the scheme is to be usable for ocean data assimilation.

(2) The analysis scheme should be flexible enough to efficiently utilize spatially variable flow-dependent background-error covariances expected from a future Ensemble Kalman Filter.

The new 3D-Var type scheme relies on 3-D physical-space spatial filters. The analysis equations are solved in model (grid) space using a preconditioned conjugate-gradient solver. The scheme utilizes spherical geometry in the horizontal and a hybrid coordinate in the vertical.

## 2 The covariance model

To obtain flexibility while ensuring positive definiteness, we define the spatial covariance model *constructively*, i.e. we build a model for the underlying random field(s). Another important issue to be addressed is computational efficiency, so we would like the covariance model to produce compactly (locally) supported correlation (or related) functions. These two features (constructive definition and local support) has led us to introduce a spatial generalization of the well-known—in the time-series theory and practice—ARMA (auto-regression moving average) model. In the one-dimensional case, ARMA models proved to be very efficient in modelling many realistic random processes, so that in most situations the orders of both AR and MA digital filters estimated from real data appeared to be very small. Small orders imply small supports of the impulse response functions for the respective filters, hence, both AR and MA operators can be represented by very sparse matrices. This is of primary importance for our practical data assimilation system in view of huge dimensionality of atmospheric and oceanic data assimilation problems. The resulting SARMA (spatial ARMA) model writes in the space-continuous form:

$$S\xi = V\alpha, \quad (1)$$

where  $\xi$  is the background-error field,  $\alpha$  denotes the white noise,  $S$  is the SAR filter (linear integral operator), and  $V$  is the SMA filter.

In this article, we consider the 2-D univariate problem on the sphere  $S^2$ . We develop an isotropic model, which is to be used as a building block in the future real implementation. Isotropy implies that each of the two operators,  $S$  and  $V$ , in Eq.(1) is defined by its generating radial function,  $s(\rho)$  and  $v(\rho)$ , respectively, where  $\rho$  denotes the angular distance, e.g. for  $S$ :

$$(S\xi)(x) = \int_{S^2} s(\rho(x,y))\xi(y)dy, \quad (2)$$

where  $x$  and  $y$  are points on the sphere and  $dy$  the area element. In order to use the above SARMA model in the analysis scheme, we discretize the supports of the random fields  $\xi$  and  $\alpha$ , getting

$$\mathbf{S}\vec{\xi} = \mathbf{V}\vec{\alpha}, \quad (3)$$

---

<sup>1</sup>Corresp. address: tsyraulnikov@mecom.ru

where  $\mathbf{S}$  and  $\mathbf{V}$  matrices are easily derived from the generating functions  $s(\rho)$  and  $v(\rho)$  and  $\vec{\alpha}$  is the unit-variance white-noise vector. Hence, the background-error covariance matrix is

$$\mathbf{B}_\xi = \mathbf{W}\mathbf{W}^*, \quad \text{where} \quad \mathbf{W} = \mathbf{S}^{-1}\mathbf{V}, \quad (4)$$

The great advantage of the above *constructive* model formulation is that we are free to change matrices  $\mathbf{S}$  and  $\mathbf{V}$  in any way (to account for spatially variable background-error statistics) without a danger to lose well-posedness of the model.

### 3 Estimation of the SARMA model

Having an estimate,  $B^{emp}(\rho)$ , of the true covariance function,  $B(\rho)$ , we seek functions  $s(\rho)$  and  $v(\rho)$  such that: (i) the implied model covariance function is close to the empirical one, and (ii) both  $s$  and  $v$  have as small supports as possible. A variational formulation is used to solve this problem. Some results for two correlation functions estimated at DWD (Anlauf et al.2005) are shown in Fig.1.

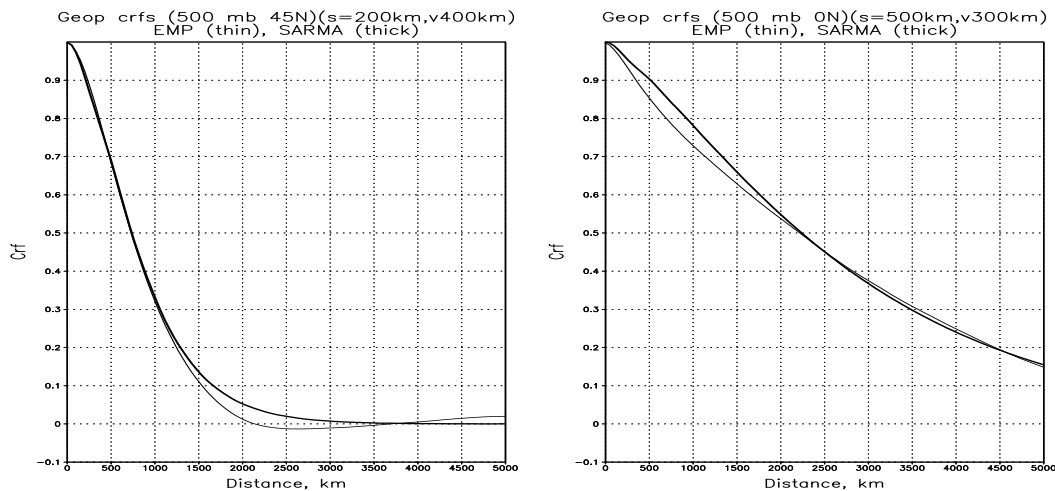


Figure 1: Empirical (thick) and model (thin) correlation functions for 500-hPa geopotential errors. *Left*: Latitude 45N. Supp(s)=200 km, Supp(v)=400 km. *Right*: Latitude 0. Supp(s)=500 km, Supp(v)=300 km.

One can see that very small supports ( $\leq 500$  km) of functions  $s$  and  $v$  appeared to be sufficient to accurately approximate quite broad correlations. Small supports imply that both  $S$  and  $V$  matrices are very sparse, which is of paramount importance for the computational analysis algorithm.

### 4 Conclusions

The new 3D-Var type assimilation scheme is under development in the Russian Hydrometcentre. The scheme is based on the spatial ARMA filters. Work on the numerical solver and the observational (in situ and satellite) processing scheme is in progress. Currently, a 2-D univariate version of the scheme is tested with synthetic observations.

We would like to thank H.Anlauf, who kindly provided us with the empirical correlations. This study has been supported by the Russian Foundation for Basic Research under grant 04-05-64481.

### References

Anlauf H., Wergen W. and Paul G. A study of the flow-dependence of background error covariances based on the NMC method. – Res. Act. Atm. Ocean. Modelling, WMO, 2005, Rep. N 35, pp. 1.1–1.2.